J Therm Spray Tech (2022) 31:780–817
https://doi.org/10.1007/s11666-022-01379-z

REVIEW

# The Bonding Formation during Thermal Spraying of Ceramic Coatings: A Review

**Chang-Jiu Li[1] · Xiao-Tao Luo[1] · Shu-Wei Yao[2] · Guang-Rong Li[1] · Cheng-Xin Li[1] · Guan-Jun Yang[1]**

Submitted: 20 October 2021 / in revised form: 15 December 2021 / Accepted: 16 December 2021 / Published online: 6 April 2022


**Abstract** Thermal spraying is the most important coating technology for depositing advanced ceramic coatings which have been widely applied to different industrial fields for materials protection and various physical–chemical functions. The adhesion and cohesion are of primary importance for the successful applications of ceramic coatings. Three bonding mechanisms contribute to the enhancement of the adhesion and cohesion, including mechanical interlocking, physical bonding and chemical bonding. It is still challenging to achieve chemical bonding in thermally-sprayed coatings. In this paper, the main factors influencing the bonding formation during thermal spraying of ceramic coatings, including spray particle parameters and substrate parameters, are examined from splat formation to coating formation to find solutions to the above challenge. The research progress on splat formation revealing characteristic dynamic parameters relating to the bonding formation kinetics will be briefly presented for the key factors determining splat shape, flattening time, solidification time, cooling rate, interface temperature, and transient dynamic contact pressure during flattening. The typical coating lamellar structure features with limited intersplat bonding less than one-third for refractory ceramics, which dominate the coating properties and performance based on theoretical relationships between the microstructure and properties, are presented. The effects of spray particle parameters on the intersplat bonding reveal that the bonding ratio is increased with increasing particle temperature, but decreased with increasing particle velocity which benefits only the mechanical bonding. Most importantly, recent studies have revealed that the liquid splat–substrate interface temperature higher than the glass transition temperature of spray materials is a necessary and sufficient condition for splat bonding formation. A critical bonding temperature concept is proposed to control the intersplat bonding formation by controlling the substrate preheating temperature. The critical bonding temperature is related to the melting point of spray materials. A model is proposed to understand the effect of the interface temperature on the bonding formation of impacting liquid splat and the bonding mechanisms. The condition for certain ceramic spray materials to form a bulk-like dense coating with the intersplat interface completely bonded becomes well understood. Moreover, the effect of metal substrate oxide scale control on the adhesion reveals that an adhesive strength higher than 100 MPa can be achieved for plasma-sprayed ceramic coatings. The excellent bonding at the interface between the splat and the oxide scale pre-oxidized on the metal substrate can be also explained by the bonding formation model. It becomes possible that, through both the controls of the pre-oxidation and the deposition temperature, all the interfaces in the ceramic coating with the metal/oxide-scale/splat/splat system can be bonded by chemical bonding to achieve an excellent load-bearing ceramic-coating system.

This invited article is part of a special issue focus in the Journal of Thermal Spray Technology celebrating the 30th anniversary of the journal. The papers and topics were curated by the Editor-in-Chief, Armelle Vardelle, University of Limoges/ENSIL.

✉ Chang-Jiu Li
licj@mail.xjtu.edu.cn

[1] State Key Laboratory for Mechanical Behavior of Materials, School of Materials Science and Engineering, Xi'an Jiaotong University, Xi'an 710049, Shaanxi Province, People's Republic of China

[2] National Key Laboratory of Science and Technology on High-strength Structural Materials, Central South University, Changsha 410083, China

**Keywords** adhesive strength · ceramic coating · cohesion · critical bonding temperature · interface bonding · intrinsic bonding temperature · thermal spray

## Introduction

Ceramic coatings have been widely employed as protective coatings and functional coatings to endow material surfaces with various special functions (Ref 1-3). As protective coatings, they have been used for thermal insulation, electrical insulation, and for wear and corrosion resistance. Ceramic coatings include oxides, carbides, borides, nitrides, and silicides, as well as several glass materials (Ref 4, 5). Advanced ceramic coatings are usually fabricated by thermal spraying, physical vapor deposition (PVD), chemical vapor deposition (CVD), and spraying/dipping, sol–gel, micro-arc oxidation, and laser-assisted deposition. Among these processes, statistical data has shown that thermal sprayed ceramic coatings take about two-thirds of the market share of advanced ceramic coating applications in North America (Ref 6). Therefore, thermal spraying of ceramic coatings has been the essentially important ceramic-coating manufacturing technology in modern industries.

A thermal spray ceramic coating is formed by the stacking of pancake-like splats, resulting from rapid cooling and solidification following successive impacts of a stream of molten or semi-molten spray droplets. Accordingly, a thermal spray ceramic coating presents a lamellar porous structure. For all coatings, having a high enough adhesion is essential for them to be successfully applied to different engineering applications (Ref 4, 5, 7, 8). Then, the cohesion between the splats dominates the performance of the ceramic coatings along with the pore structure (Ref 9-11). For the development of high-performance coatings, it is necessary to better understand the factors dominating the bonding formation and related bonding mechanisms.

Generally, the adhesive strength is contributed by one or more than two of the following bonding mechanisms: mechanical bonding, physical bonding, and chemical bonding or metallurgical bonding between the metallic substrate and the ceramic splat interface (Ref 4, 7, 12, 13).

It is well known that roughening a substrate surface is a primarily necessary process for thermal spray ceramic coatings of good adhesion, and that the topography of the substrate surface significantly influences the adhesion of thermal spray coatings. Therefore, mechanical interlocking plays an essential role in coating adhesion. High-impact transient pressure at the interface between the molten splat and the solid substrate interface enhances the filling of the melt into capillary cavities on the surface, and subsequently the coating adhesion by mechanical interlocking (Ref 12, 13). The high pressure also enhances the intimate contact of the splat atoms with these substrate, which benefits the physical bonding between a metal substrate and the ceramic splats through van der Waals forces. For metallic coatings, a high-temperature molten droplet impact can cause the melting of a local substrate and the forming of metallurgical bonding at the substrate/coating interface (Ref 14-20). In the case of ceramic coatings, local interface multi-component ceramic phase formation implies the melting or a local interaction to form a strong adhesive bonding (Ref 4). Such an effect much depends on the physical and thermal contact conditions of the impacting spray particles with the underlying substrate. Since the thermal conductivity of metals is larger than those of oxide ceramic coating materials, the splat in intimate contact with a preheated substrate experiences a much higher cooling rate than 3-6 $\times$ $10^8$ K/s, giving a very limited time, less than 10 μs, for the splat to stay liquid to wet the substrate surface (Ref 21-24). Fortunately, an oxide scale forms on a metallic substrate surface, being favored for ceramic splats to bond with. However, the diverse combinations of a substrate with a ceramic coating seem to make the adhesive bonding mechanisms very complex. To understand the adhesion, not only the substrate surface topography but also the chemistry of oxide scales should be well addressed (Ref 1).

The cohesive strength of ceramic coatings depends on the intersplat bonding quality, which dominates the mechanical properties and the thermal and electrical transport properties of the coating, and so on (Ref 9-11). Since the bonding is evolved when the sprayed molten particles are deposited on the previously deposited splat surface with the same material, the factors influencing the bonding formation within ceramic coatings are less than that for adhesive bonding. The main factors include the spray particle parameters, such as temperature, velocity, and size, and also their distributions, as well as the substrate surface parameters, such as temperature and topography. It was generally believed that the higher the particle velocity, the higher the cohesion which could be attributed to a high interface bonding ratio. Higher particle velocity impact brings a more intimate contact of spreading spray particles with the splats underneath by higher dynamic pressure (Ref 13, 25, 26). Moreover, this was largely evidenced by the fact that D-gun coatings presented higher adhesion and superior wear performance over plasma-sprayed counterparts (Ref 12). On the other hand, the higher the particle temperature, the higher the lamellar bonding ratio is expected, since a higher droplet temperature may lead to a high-contact interface temperature of the current molten splat with the previously solidified underlying splats. Therefore, the bonding enhancing mechanism

by a higher particle temperature should be different from that by the increased particle velocity. It is generally easier to achieve a high particle velocity by using high-velocity processes such as D-gun (Ref 27, 28) and high-velocity oxygen fuel spray (HVOF) (Ref 29). However, since the effort to increase the particle velocity may limit or reduce the particle temperature, it is generally difficult to simultaneously raise the velocity and the temperature of the spray particles. Thus, it is important to understand the individual contributions of particle temperature and velocity to different mechanisms to make a proper strategy for the optimization of the spray process parameters. Many investigations have been concerned with the effect of substrate temperature on the ceramic coating microstructures with emphasis on the effect of intersplat bonding (Ref 30-42). A recent study revealed that the deposition temperature, being referred to as the coating surface temperature before molten droplet impact or the substrate temperature, is the most important factor to determine the intersplat bonding formation during ceramic coating deposition (Ref 43, 44). Through controlling the deposition temperature, a complete chemical bonding through the whole ceramic splat interface can be achieved. Moreover, the coating microstructures may be designed and created on the application performance need basis through the control of particle melting state and deposition temperature (Ref 45).

Therefore, in this review paper, the dominant factors over adhesive and cohesive bonding of thermal spray ceramic coatings will be presented starting from the splat formation showing the characteristic parameters. These parameters are essential to understand the fundamental features relating to the bonding formation kinetics. The general features of lamellar structure of the ceramic coatings with limited intersplat bonding will be demonstrated. The effect of spray particle velocity and temperature on the bonding formation is reviewed. The main focus is on the research progress on the impact of deposition temperature and consequently liquid splat–substrate interface temperature on the bonding formation achieved by substrate preheating to understand the dominant factors for intersplat bonding formation and subsequent bonding mechanisms.

## Typical Characteristic Parameters for Bonding Formation Inherent in Thermal Spraying

### Morphology of Splats

The bonding formation during thermal spraying includes the formation of adhesion and cohesion. The adhesion usually refers to the bonding between a ceramic coating and a metallic substrate. Thus, the adhesion formation involves the interface between two different materials, while cohesion is concerned with the bonding formed at the interfaces between adjacent splats within the coating, which involves the interface between identical materials. Based on the coating formation theory, rapid radial spreading on the substrate, rapid cooling, and solidification following the impact of molten droplets are the basic processes for the formation of thermal spray coating. Accordingly, through these processes, individual splats are formed and subsequent successive stacking of splats forms the coating. At the same time, the bonding forms during the individual splat formation process. Therefore, the investigation into splat formation is the primary step to understand the critical parameters influencing bonding formation kinetics (Ref 46).

The morphology of the splat influences the adhesion/cohesion. Splashing is frequently observed during splat formation, which results in weakly adherent radial arms or small particles. It has been well understood through intensive investigations during the last three decades that the preheating temperature of the substrate surface dominantly affects the splat morphology (Ref 44-52), as well as other features such as splat–substrate thermal contact (Ref 53, 54), and so on. When splats are deposited on a polished flat substrate with adsorption of moisture and/or other evaporable adsorbates in an ambient atmosphere, the resultant splats present irregular shapes without following any law but with random irregularity (Fig.1b) (Ref 52, 55, 56). On the other hand, when the substrate is preheated to remove all surface-adsorbed moisture and/or other adsorbates, a regular disk splat is usually acquired on a clean flat substrate (Ref 48-52), provided that the Reynolds numbers of the molten droplets are lower than about 50,000 (Ref 57, 58). Here, the disk splat represents the splats in a disk shape with few radial arms observed. For most ceramic spray materials, this condition for the above Reynolds numbers can be fulfilled (Ref 48, 59-61). Generally, the splats deposited on a polished flat substrate with preheating to a temperature higher than 150 °C or the critical transition temperature present a regular disk shape (Fig. 1a) (Ref 61, 62).

### The Size of Regular Disk Splat

The size of regular disk-like splats depends on the parameters of the spray molten droplets, i.e., velocity, temperature, and size, and the thermal interaction of the molten droplets with the substrate, leading to a restrictive effect of rapid solidification on the spreading. The size of the splat is usually characterized by the flattening ratio, being defined as the ratio of disk splat diameter ($D$) to the initial droplet diameter ($d$). The flattening ratio ($\xi$) can be

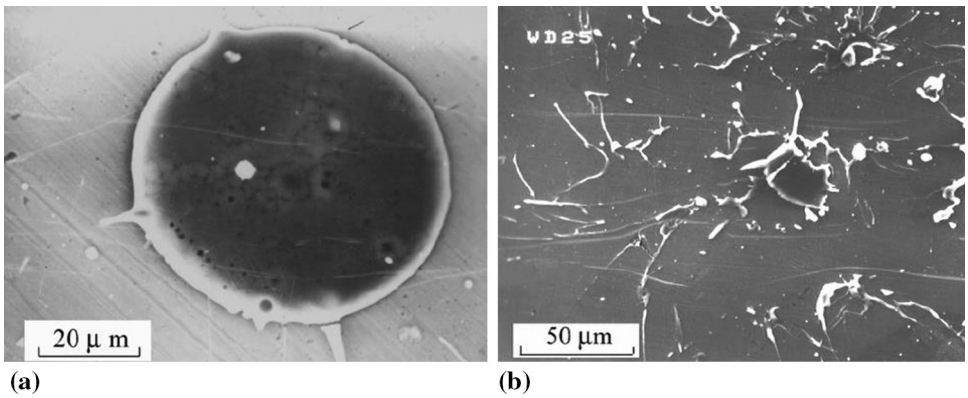


**Fig. 1** (a) Regular disk-like $Al_2O_3$ splat deposited on a preheated flat stainless steel surface (150 °C); (b) $Al_2O_3$ splat deposited at room temperature on a polished flat stainless steel surface, showing irregular shape caused by splashing during spreading (Ref 52). Reprinted with permission from Elsevier

correlated to the Reynolds numbers of molten droplets (*Re*), as (Ref 21, 63):

$$\xi = a\mathrm{Re}^b \qquad \text{(Eq 1)}$$

where $a$ and $b$ are constants. They can be acquired by theoretical modeling, which gives the exponential constants of 0.125 (Ref 64) and 0.2 (Ref 63). The constant a can also be given by the regression of the data obtained by simulation, supposing $b = 0.2$ (Ref 65-68) or experiments with $b = 0.125$ (Ref 69). The Reynolds numbers (*Re*) is expressed as:

$$\mathrm{Re} = \frac{\rho_p d_p V_p}{\mu_p} \qquad \text{(Eq 2)}$$

where $\rho$ is the density, $d$ the droplet diameter, $V$ the particle velocity, and $\mu$ the viscosity of the droplets which is determined by the droplet temperature. The subscript $p$ represents the parameters of the spray particle.

In the ideal case of forming a regular disk splat after a molten droplet impacts on a substrate, the diameter of a regular disk splat depends on the flattening degree and the original particle size, as shown in the above equation. The flattening degree increases and subsequently the splat thickness decreases with the increase of particle velocity and temperature, while the experimental results revealed that the flattening degree of ceramic droplets ranges from 3 to 5 for most ceramic spray materials and spray conditions (Ref 70). This corresponds to a splat thickness from 0.5 to 3 µm.

### Time from Impact to Complete Solidification

For a flat substrate, the formation of the bonding during splat formation, consisting of physical and chemical bonding, theoretically depends on the interaction between the atoms or molecules in the molten splat with the atoms in the substrate. Accordingly, the primary parameters dominating the bonding formation include splat–substrate contact condition, interface temperature evolution, transient pressure of spreading melt exerted on the substrate at the interface, and the time available for reaction.

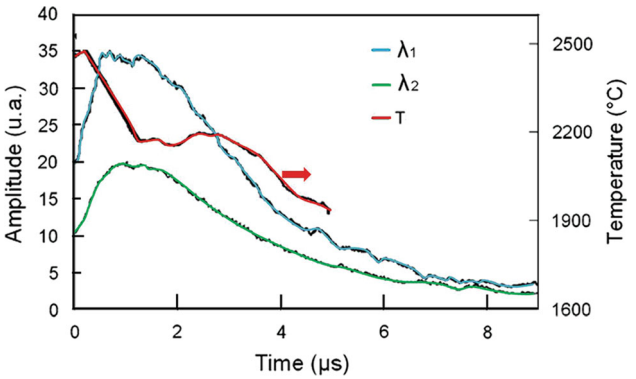


**Fig. 2** Evolutions of the thermal emission intensities of the detectors with different wave lengths and the splat surface temperature against the time immediately after molten spray particle impact (Replotted based on Ref 76)

Molten droplet impact is typically concerned with splat cooling, which involves rapid solidification and quenching (Ref 4, 71-73). The thermal contact between the spreading melt and the substrate determines the heat transfer, the splat–substrate interface temperature, and subsequently the kinetics of all the processes in the cooling process. Through developing a delicate thermal emission detection pyrometer system for monitoring the temperature of spreading splat (Ref 74), flattening and cooling processes of molten droplets impacting on a substrate can be examined (Ref 23, 24, 54, 59, 60, 75). Combined with a fast camera, the flattening process can be examined through imaging (Ref 24, 76). Figure 2 shows a typical change of the signals from two detectors with different wave lengths and the splat surface temperature (Ref 76). The time from the impact to the rapid rise of the signal amplitude to the maximum corresponds to the flattening time, while the evident plateau on the cooling curve corresponds to the solidification time. Therefore, the flattening time, the solidification time, the cooling rate, and the cooling time, defined as cooled to about 800 °C, have been estimated.

Through modeling and comparing with the observed temperature change (Ref 48, 53), the thermal contact resistance at the splat–substrate interface can be obtained. When a spray molten droplet impacts on a preheated substrate with complete removal of surface adsorbates, the thermal contact is nearly perfect at the interface between the spreading melt and the substrate with a thermal contact resistance being lowered to $10^{-7}$–$10^{-8}$ $m^2$ K/W (Ref 48, 53, 54).

For common ceramic spray particles, the flattening time is about or less than 1 μs (Ref 48, 76). Then, the time from impact until complete solidification being characterized from the cooling curve (Fig. 2) is less than 10 μs. The solidification time is certainly dependent on splat thickness and interface contact quality, and substrate material properties. It increases with the increase of the splat thickness, as shown in Fig. 3(a) (Ref 48). For ideal cooling, the cooling rate is inversely proportional to the square of the splat thickness (Ref 71). Therefore, with increasing molten spray particle temperature and velocity, the cooling time decreases and thus the cooling rate is significantly increased due to a decrease of splat thickness, as shown in Fig. 3(b). These facts mean that the available time for impacting molten droplets to form the bonding with the underlying substrate through liquid wetting and reaction is generally less than 10 μs. Therefore, the bonding through the reaction of the atoms in the liquid molten splat with the atoms in the solid substrate should be completed in a very short time of a few microseconds.

The cooling rate also depends on the heat sink effect of the substrate (Fig. 4). In the case of a yttria-stabilized zirconia (YSZ) splat deposited on a stainless steel substrate, the cooling rate is from 400 to 1000 °C/μs (Ref 48). When the substrate is changed to an atmospheric plasma-sprayed (APS) YSZ coating, the cooling rate decreases to about 100 °C/μs due to the low thermal conductivity of the YSZ substrate. The former is concerned with adhesion formation, while the latter is related to cohesion formation. A higher cooling rate leads to a shorter time available for the interaction of the molten ceramic splat with the substrate, indicating more difficulty for a strong adhesion formation than cohesion. As will be shown later by the latest research results, through controlled oxidation of the substrate to form a ~1-μm-thick well-adherent oxide scale, a significant increase of the adhesive strength to 105 MPa was obtained for an APS alumina coating on polished Ni (Ref 77). This can be partially attributed to the increase of the substrate surface layer thermal resistance. This oxide scale on the Ni substrate possibly reduces the cooling rate and then increases the solidification time and consequently the liquid splat–substrate interface temperature. A poor contact with a thermal contact resistance of $10^{-6}$ $m^2$ K/W or higher was observed for molten droplet impact on a cold substrate in an ambient atmosphere (Ref 48, 54, 76). The cooling rate is reduced by a factor of about 10 (Ref 54) and the solidification time becomes much longer, due to a gas cushion under the melt which causes melt instability and

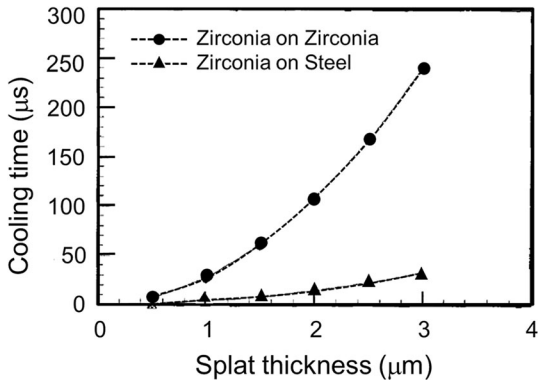


**Fig. 4** Effect of the substrate material type on the splat cooling time. The change from the metal to the ceramic substrate leads to the increase of the cooling time by a factor of two orders (Replotted based on Ref 48).

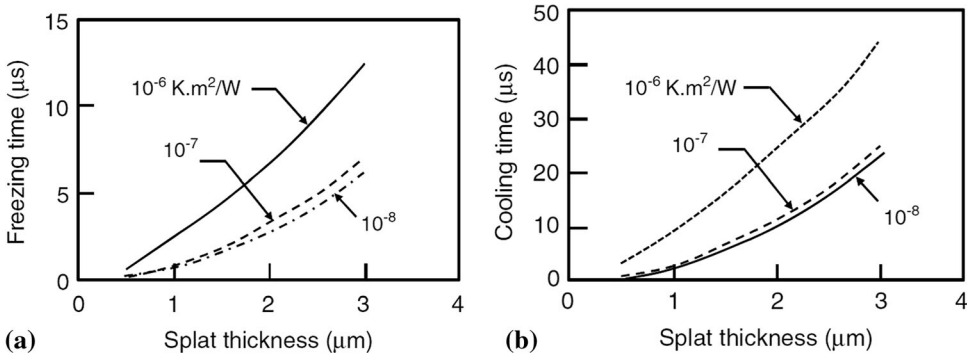


**Fig. 3** Relationships between the splat thickness and the splat solidification time (a) and cooling time (from impact to cool to about 800 °C) (b) for yttria-stabilized zirconia (YSZ) at different thermal contact conditions; $10^{-7}$–$10^{-8}$ K $m^2$/W means the perfect contact corresponding to the preheated substrate conditions with surface adsorbates removed, while $10^{-6}$ K $m^2$/W corresponds to the splat cooling condition without substrate preheating (Replotted based on Ref 48)

subsequent splashing (Ref 54). Unfortunately, this long time does not contribute to the bonding formation. It should be kept in mind that only a very short time of less than 10 μs is available for the formation of strong bonding, i.e., chemical bonding for a ceramic splat through a physical or chemical reaction. The longer this available time, the more a sufficiently thermal or chemical reaction may occur and consequently a strong bonding forms.

### Interface Temperature Evolution

The temperature at the liquid splat–substrate interface is the most important parameter to determine the bonding during splat formation regarding the very short available time. This can only be estimated by simulation. Since the flattening time of about 1 μs is less than solidification time, a one-dimensional model is used to estimate of the interface temperature (Ref 48, 53). Here, a liquid film with a given thickness equal to the splat thickness is instantaneously put on the substrate surface. The heat transfer occurs essentially in the direction of droplet impact across the interface. Heat losses from the splat surface by radiation and convection are neglected. The thermal contact model with a certain thermal contact resistance at the splat–substrate interface is employed for numerical simulation (Ref 20, 48). In this case, the temperature of the splat bottom is different from that of the top surface of the substrate when the thermal contact resistance is larger than $10^{-6}$ $m^2$ K/W. To form the bonding, the real contact between the liquid splat and the substrate should take place, in which the thermal contact resistance should be so small that can be neglected. In such a case, the temperature of the splat bottom is approximately equal to that of the top surface of the substrate, being referred to as the interface temperature. The comparison of the simulated splat surface temperature with that of the observed one shows reasonable agreement (Fig. 5, Ref 48), suggesting the feasibility of the one-dimensional model. Such a model was used to estimate whether a molten droplet impact causes the melting of substrate for metal splat deposition or solidification of the molten splat as the phase transitions from liquid to solid (Ref 20, 78, 79). The early investigations were concerned mainly with the adhesion formation by focusing on the interaction of the molten droplets with the real substrate with a heterogeneous interface (Ref 20). The recent investigations are more oriented to examine the intersplat bonding formation by using splat identical to a substrate, such as a NiCrBSi droplet impacting on a NiCrBSi substrate (Ref 78, 79). The results showed that the interface temperature depends on both the droplet temperature and the substrate temperature. The modeling successfully predicts the conditions for the molten droplet impact-induced substrate melting for metal coating deposition. However, few publications have been found that investigate the effect of the interface temperature on the bonding formation without substrate melting by simulations (Ref 44, 48, 53, 80). With sprayed γ-alumina as the substrate, the substrate temperature increases up to 1600 K when an alumina droplet with a temperature of 2800 K impacts on a substrate preheated to 573 K under the assumption without undercooling (Ref 80). For a 1-μm-thick YSZ droplet at 50 °C higher than its melting point, its impact leads to the interface temperature increasing to 927 °C for a stainless steel substrate and to 1727 °C for a YSZ substrate, indicating the significant influence of the substrate thermophysical properties on the interface temperature (Ref 48).

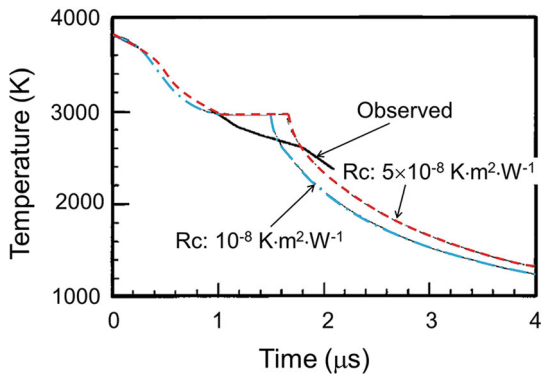


**Fig. 5** Change of YSZ splat surface temperature after impact on a steel substrate. The comparison of the simulated data with two thermal contact resistances (Rc) using a one-dimensional model with the measured surface temperature (bold line), showing good agreement. (Replotted based on Ref 48)

Moreover, the interface temperature evolution can also be simulated through computational fluid dynamics (CFD) modeling. Through the simulation of the spreading process using CFD modeling (Ref 81), it was found that impacting of YSZ particles with a temperature of 2800 °C (~50 °C over the melting point) results in the temperature increase of the YSZ substrate surface from its initial temperature of 200 °C to about 2000 °C at the splat center under good thermal contact. The interface temperature is also influenced by the substrate materials. The same above-mentioned YSZ droplet causes the temperature to increase to 900 and 400 °C at the splat center for stainless steel and copper substrates, respectively. In comparison to the results obtained by the one-dimensional model, those results may indicate that this model may underestimate the interface temperature, especially at the splat central region. Since it is evident that metal substrates have higher thermal effusivity than ceramics (for example, 9700 J/$m^2$ K $s^{0.5}$ for steel vs. 2800 J/$m^2$ K $s^{0.5}$ for YSZ) (Ref 48), the interface temperature between a ceramic splat and a metal substrate is lower than the intersplat interface temperature during ceramic coating deposition. This also reveals that it is more

difficult for a ceramic coating to form a strong adhesion than cohesion. The effect of the interface temperature on the bonding formation will be explained in more detail in a later section.

### Contact Pressure at Liquid Splat-Substrate Interface

A high contact pressure at the interface between the liquid splat and the substrate is necessary to keep an intimate contact of spreading melt with the substrate surface, and force the penetration of melt into the surface cavities on a rough substrate to ensure mechanical interlocking. Moreover, high pressure at the intimate contact region benefits not only the physical bonding formation but also a possible chemical reaction for the bonding formation. The maximum pressure ($P$) generated at the interface center upon droplet impact can be expressed by (Ref 82):

$$P = \frac{\alpha}{2}\rho_p C_{so} V_p \quad \text{(Eq 3)}$$

where $C_{so}$ is the sound velocity of molten liquid, $\rho$ the density, $V_p$ the spray particle velocity, and $\alpha$ is a constant (approximately 0.9).

The above equation is a modification to the water hammer pressure equation. For oxide ceramic materials, using $C_{so} = 5800$ m/s, $\rho = 5$ g/cm$^3$, $V_p = 150$ m/s as typical values, a maximum peak impact pressure of 5.35 GPa can be estimated. The pressure decreases very rapidly once the spreading starts. At 0.01 μs after impact, the peak pressure decreases to less than one-tenth of the maximum pressure (Ref 26). By solving the continuity equation during spreading, Sobolev et al. (Ref 83) established theoretically the pressure distribution along the splat radial direction which is related to the droplet parameters. However, the pressure is transient with the spreading of the impacting melt. Li and Li (Ref 68) examined the evolution of dynamic pressure during the spreading process through numerical simulation, giving an empirical equation for the estimation of the peak contact pressure:

$$P = 3.57\rho_p V_p^2 \quad \text{(Eq 4)}$$

For YSZ particles impacting at 150 m/s, the maximum pressure can be estimated to be 402 MPa. The simulation revealed that the maximum peak pressure decreases rapidly with the proceeding of the spreading (Fig. 6) (Ref 68). Moreover, the dynamic pressure mainly acts within the splat region less than the initial droplet diameter (Fig. 7) (Ref 68). The data show that the instant local maximum pressure decays to very low level in a splat region larger than the flattening ratio of 1.5-2. At the moment of spreading to a flattening ratio (relative radius) of 2, the pressure over the whole contact interface becomes lower

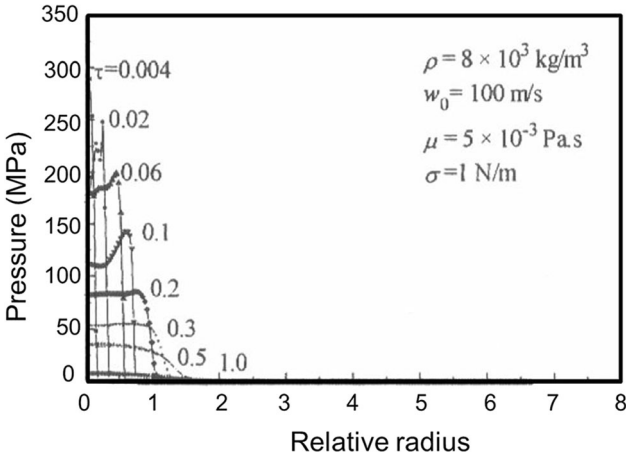


**Fig. 6** Typical change of the transient dynamic contact pressure distribution along the splat–substrate interface with flattening time (Ref 68). Reprinted with permission from Springer Nature.

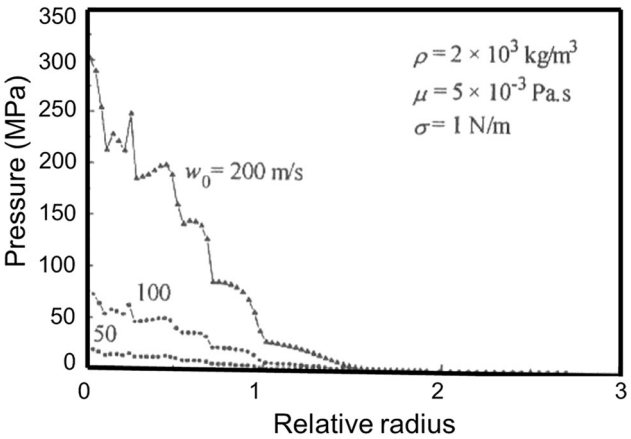


**Fig. 7** Typical maximum dynamic contact pressure experienced at different radial locations at different spray particle velocities. The data show that the instant local maximum pressure decays to very low level in the splat region larger than the flattening ratio of 1.5-2 (Ref 68). Reprinted with permission from Springer Nature.

than 0.27 MPa. Moreover, in the region $\xi > 2.5$, the maximum pressure decreases to less than 0.02 MPa (Ref 84). One important feature is that, in the region of the flattening ratio larger than 1.5-2, the contact pressure becomes less than 1 MPa (Ref 84), being less than that generated by rapid vaporization of adsorbates through rapid heating (Ref 52). This fact accounts for the size of residual splats of their central part, with all other surrounding splat material splashed away. Therefore, when the effect of the contact pressure is considered on the splat formation and then the bonding formation, it only acts effectively in the region at $\xi < 2$. For most splat substrate interface regions, no effective dynamic contact pressure acts on them. The higher the flattening ratio, the larger the splat interface region where there is no effective dynamic contact pressure. In such an interface region, the bonding

formation during spreading should depend on temperature-activated reactions.

## Effect of Substrate Preheating on the Structure of Ceramic Splats

Splat is a basic unit to construct thermal spray coatings. Its morphology significantly influences the microstructure of the resultant coating. Primarily, the morphology of the splat is determined by the interaction of impacting molten droplets with the substrate. For a certain spray material, the parameters of the spray particles influencing splat morphology include the molten degree, temperature, velocity, and size of individual spray particles. The parameters of the substrate include the morphology (or roughness), preheating temperature, and surface chemistry. For partially molten particles, its impact at a high velocity results in inevitable radial splashing and rebounding off the unmelted central solid core, leading to the formation of splat with complex and irregular shapes (Ref 55, 85). For ceramic spray materials, since the deposition efficiency increases with the melting degree of the spray powders (Ref 86, 87) as illustrated by Fig. 8, the optimization of spray conditions is usually carried out to make the spray particles as fully molten as possible. Thus, the impact of sufficiently molten spray particles is typical of the thermal spray of ceramic coatings.

The splat deposited on a flat substrate by molten droplets presents either a regular disk shape or an irregular shape, as mentioned previously. The former occurs on a clean flat surface without any evaporable adsorbates, while the latter appears when the substrate surface is adsorbed by any evaporable adsorbates (Ref 47-53). Since the substrate is usually exposed to an ambient atmosphere, and the adsorption of moisture inevitably occurs, the preheating of the substrate surface to a temperature higher than 150 °C generally completely removes the physisorption water. Accordingly, splat with a regular disk shape is deposited. Fig. 9 illustrates the YSZ splats deposited on polished stainless steel preheated to 70 and 230 °C (Ref 88). However, when a thick hydroxide scale is formed on the substrate surface either naturally or by hydrothermal treatments (Ref 89-92), it is difficult to obtain disk-shaped splats. This is because the rapid heating by the impacting molten droplets releases more water vapor from the hydroxides and causes splashing by the spreading melt. In this case, since chemical adsorption occurs, to which the adsorption energy changes with the type of hydroxides, the critical temperature for the transition of splat morphology change will vary largely according to the substrate material types (Ref 50, 52). Only under the preheating condition in which all evaporable adsorbates are completely removed, disk-shaped splats are deposited.

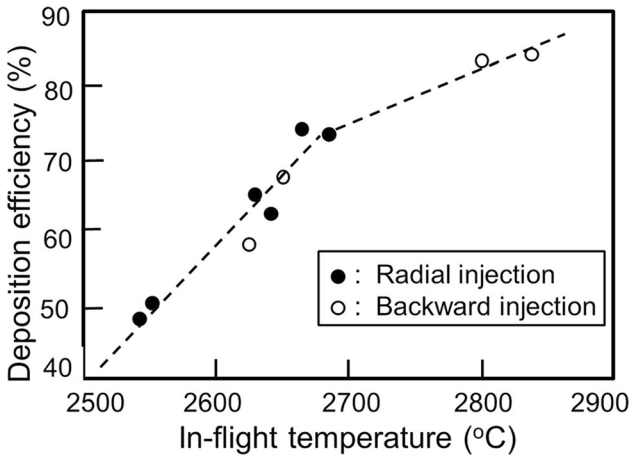


**Fig. 8** Effect of in-flight spray particle surface temperature on the deposition efficiency obtained by YSZ (Replotted based on Ref 86)

For metallic substrates, the preheating also results in the increase of oxide scale thickness in addition to the removal of adsorbates (Ref 1). When an adherent dense thin oxide scale grows uniformly on the substrate surface, the oxidation of the substrate hardly affects the shape of the splats, which present disk shapes on the preheated substrate. This is typical for stainless steel (Ref 70, 93-95). When oxide scale with a rough morphology forms on the substrate surface as a low carbon steel or a low alloy steel due to different oxidation kinetics of pearlite and ferrite, the gases in the surface cavities into which the impacting droplet melt cannot enter will cause the splashing (Ref 93, 96, 97). The resultant splats present extensively fingered shapes or even with bubbles in them due to the absorption of gas and then release during solidification. The gas at the interface hinders the direct contact of the liquid splat and the substrate.

The microcrack formation is inherent to thermally-sprayed ceramic splats (Fig. 9) (Ref 88). Such intrasplat cracks result from high quenching stress during splat cooling (Ref 98). Cracking is the only way to release high quenching stress for brittle ceramic splats (Ref 99). The significant reduction of quenching stress-induced cracks occurs when the preheating temperature is higher than 900 °C for YSZ, since it was observed that, at higher preheating temperatures, the spacing between the cracks significantly increase (Fig. 10) (Ref 88). As a result, crack-free splat at a diameter of $\sim$15 μm can be observed at certain high deposition temperatures.

## Effect of Substrate Roughness on the Structure of Ceramic Splats

Practically, thermal spray coatings are applied on a blasted rough substrate surface to enhance mechanical bonding.

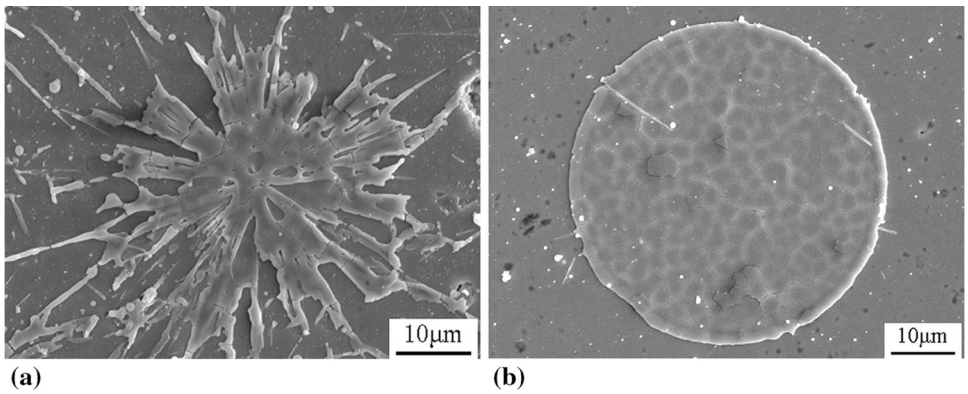


**Fig. 9** Typical morphologies of YSZ splats deposited on polished flat stainless steel substrates preheated to 70 °C (a) and 230 °C (b)

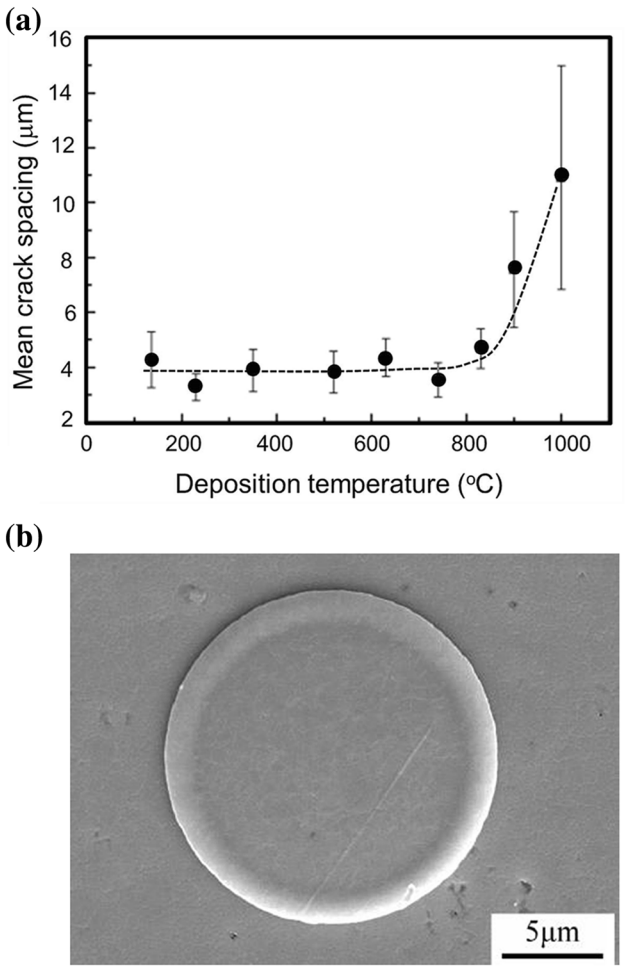


**Fig. 10** The effect of preheating temperature on intrasplat microcrack spacing (a) (Replotted based on Ref 88) and an intracrack free splat (b) deposited at a preheating temperature of 900 °C

Splat deposition tests have revealed that significant splashing occurs when molten spray droplets impact a blasted rough substrate at high velocity (Ref 100, 101). However, the splats on a preheated substrate are different from those on a cold substrate, even after the blasting. Bianchi et al. reported that alumina splat on a preheated rough substrate was rather compact with fewer cracks, due to better accommodation of thermal strain and a few pores, possibly resulting from entrapped gas, while alumina splat presented a more distorted shape with a lack of materials at the center in the case of a cold substrate, which was splashed away due to lack of adhesion. Taking account of the splat region where the effective dynamic pressure acts, the relative size of the so-called residual splat deposited on a blasted surface is less than $\xi < 2$ (Ref 68). The splat deposition on an artificial regularly ridged surface formed by planing revealed that splashing occurs because the spreading melt lacks dynamic contact pressure pushing the melt following the substrate and losing substrate support when the molten material flows over the ridge peaks. Figure 11 shows typical microphotos of Cu splats collected on the ridged stainless steel surface with preheating to eliminate the adsorbates effect. The splats in Fig. 11(c–g) were arranged in such order that five splats were formed by molten droplets that they impacted at five different locations of a–e in Fig. 11(a), respectively, as shown in the schematic. The inter-spacing of two adjacent ridges is 240 μm. When a splat is deposited on a flat substrate, it flattens to a diameter from 350 to 400 μm. Thus, the deposition of each Cu splat will stride across at least one ridge. Accordingly, the effect of a rough peak or ridge on the splat morphology can be examined. When the droplet impacts just on the ridge peak, as shown in Fig. 15(g) a uniform spreading symmetrically downward over two slopes occurs, resulting in a symmetrical saddle-like splat tightly riding on the ridge. When the impact point is located at a position near a valley, such as a and b, an upward spreading occurs and the splat material spreading over the ridges apparently splashes away. However, when the impact points are near the ridge, such as c and d, the splat materials spread over the ridges and still flatten down the slope. This is possibly due to the effective dynamic pressure exerted on the spreading liquid. Figure 12 shows images of alumina splats with a smaller size than copper splats deposited on a similar ridged surface. The same

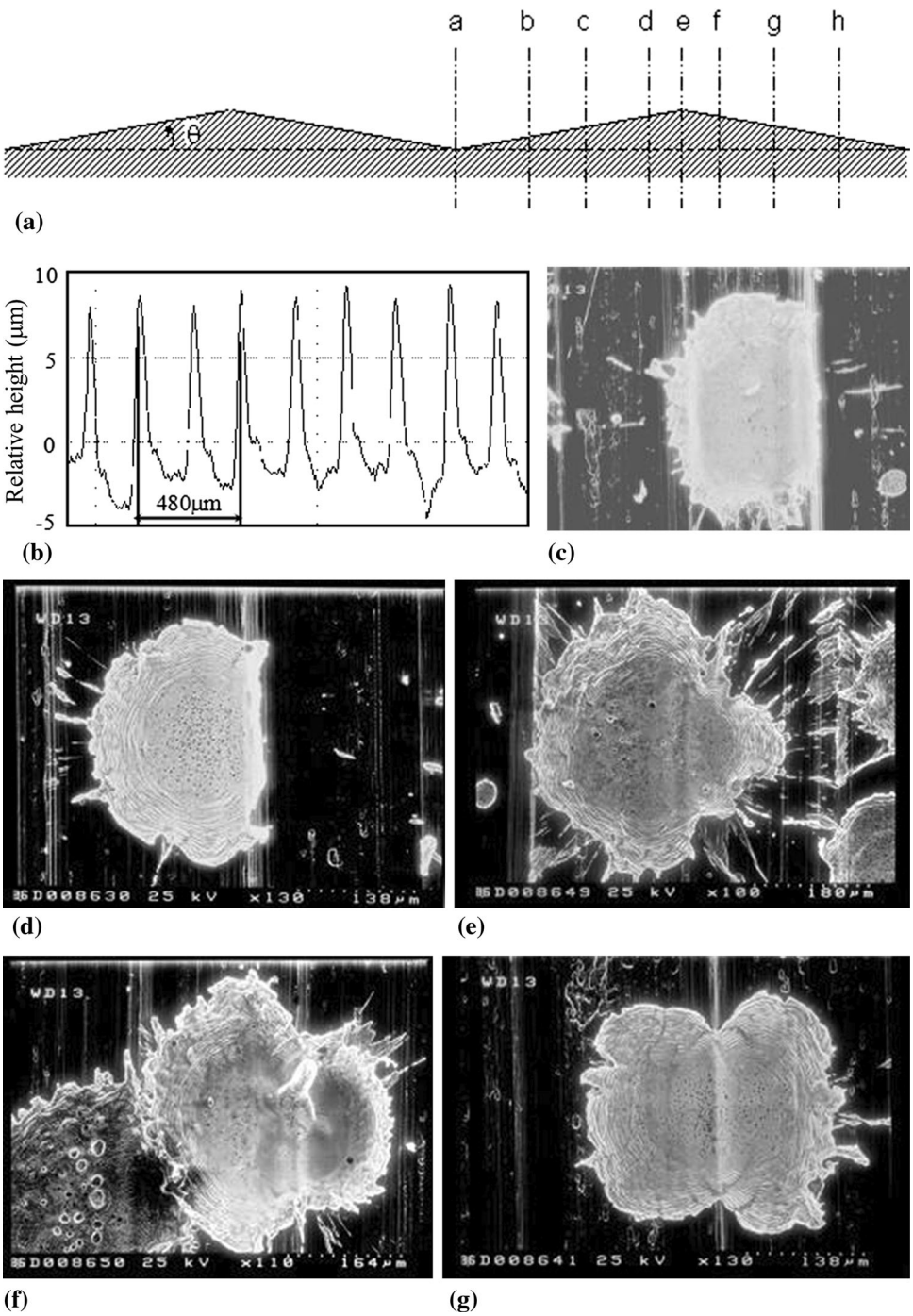


**Fig. 11** Splashing during spreading of a Cu liquid splat impacting on a nonflat surface planing to the ridged morphology as the ridged substrate surface model: (a) schematic of substrate cross-section; (b) profile of the substrate along the plane perpendicular to the ridges, showing uniform spacing of 240 μm between two ridges; the morphology of typical splats (c–g) deposited by impacting molten droplets at the locations of a–e, marked in (a) in sequential order from left to right on a substrate preheated to 350 °C

phenomena occur in the alumina splats. The impact near the ridge results in a saddle-like splat riding on the ridge. The shrinkage of the splat riding across the ridge during rapid cooling enhances the interlocking effect to the substrate ridge for such a splat. On the other hand, the impact of molten alumina at a position near the valley acquires a disk-shaped splat, but without any mechanical interlocking effect due to a relatively small size of splat to ridge spacing. The impact at the location one particle diameter away from the ridge makes the molten melt spread over the ridge but without effective dynamic pressure to push the spreading melt down to keep contact with the substrate. As a result, the melt flows over the ridge and jets away through splashing. Thus, the effective mechanical interlocking depends on the relative ratio of splat size to peak spacing on the rough surface. Taking account of the fact that the effective size of splats adhered to a rough substrate is less than two times the spray particle size, when the substrate is

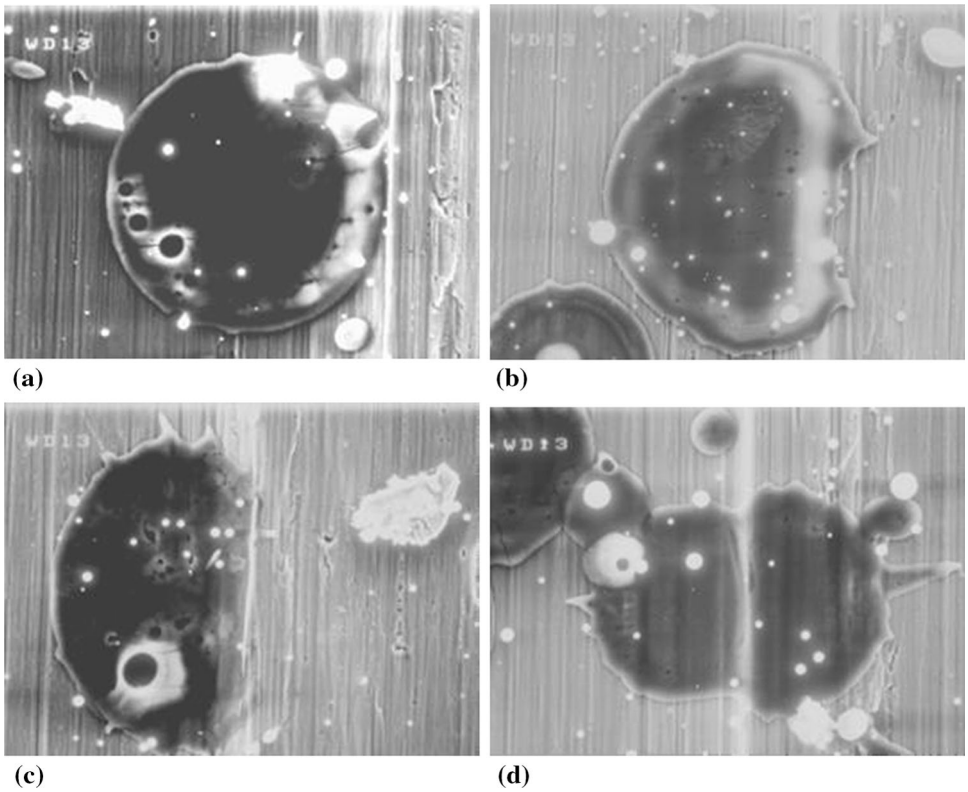


**Fig. 12** Morphology of typical splats showing splashing during spreading of $Al_2O_3$ liquid splats over the ridge peak impacting on the model surface shown in Fig. 11 at the locations marked as b, c, d, e corresponding to splats in (a), (b), (c) and (d), respectively. The splats were deposited at a preheating temperature of the substrate of 350 °C

roughened to make the adjacent peak spacings less than two times the droplet size, a coating with a strong mechanical adhesion may be formed.

## Factors Dominating the Adhesive Bonding of Ceramic Coatings

### Low Adhesion of the Common Thermal Spray Ceramic Coatings

Ceramic coatings are mostly applied to a metal surface to endow the metal substrate with excellent properties and performance. The coatings should have enough adhesive strength to avoid delamination or spallation under service conditions. The adhesion of thermal spray ceramic coatings has long been a concern. Gerdeman and Hecht summarized the adhesive strength of thermally-sprayed ceramic coatings reported up to the beginning of the 1970s (Ref 4). Pawlowski collected adhesive strength data from the literature up to the beginning of the 1990s (Ref 5). Matejka and Benko also collected adhesive strength data in their book (Ref 7). Those data are recompiled in Table 1. Typical plasma-sprayed ceramic coatings have presented adhesions of 7, 7.2, 10–11, and 7–14MPa for $Al_2O_3$, $BaTiO_3$, $ZrO_2$ , and $ZrSiO_2$, respectively. Rokide flame-sprayed ceramic coatings presented the adhesion of 7-8 MPa. (Ref 4). The ceramic coating applied to the metallic substrate directly presents an adhesion of about 10 MPa. It can be seen that, by applying a metallic interlayer as the bond coat, most ceramic coatings presented an increased adhesive strength up to over 60 MPa. The low adhesive strength, being in a range from less than 10-60 MPa, indicates that the adhesive strength of thermally-sprayed ceramic coatings is mainly contributed by the mechanical bonding (Ref 7), which relies on the mechanical interlocking of the deposited splats on a blasted rough surface. Therefore, the adhesive strength increases with the substrate roughness (Ref 100, 101). The interlocking depends on the relative ratio of splat size to average peak spacing of asperities on a rough surface, as seen in Fig. 11 and 12. It was usually revealed that splashing occurs when a molten droplet impacts a blasted rough surface. Although the residual central part of the splat adheres to the substrate under high contact pressure, splashing leads to the forming of weakly bonded radial arms and small spherical particles, reducing the adhesion of the coating.

### Effect of Substrate Oxide Scale

To promote an intimate contact between the coating and the substrate to enhance the bonding, the substrate surface should be clean without any adsorbates or condensates. The preheating is generally applied to remove the absorbates

**Table 1** Typical data for adhesive strength of different ceramic coatings

| Coating | Substrate | Bond coat | Adhesion (MPa) | References |
|---|---|---|---|---|
| $ZrSiO_4$ | 35NiCr18 | NiCr | 28.4 | (Ref 7) |
| $ZrSiO_4$ | 17346 steel | NiAl | 0.61 | (Ref 7) |
| $Al_2O_3$+2.5% $TiO_2$ | 11373 steel | No | 6.27 | (Ref 7) |
| $Al_2O_3$+2.5% $TiO_2$ | 11375 steel | NiCr | 10.63 | (Ref 7) |
| $Al_2O_3$+3% $TiO_2$ | 35NiCr18 | NiCr | 9.02 | (Ref 7) |
| $Al_2O_3$+3% $TiO_2$ | 35NiCr18 | NiAl | 18.6 | (Ref 7) |
| $Al_2O_3$+13% $TiO_2$ | 11373 steel | No | 10.7 | (Ref 7) |
| $Al_2O_3$+13% $TiO_2$ | 11373 steel | NiCr | 11.3 | (Ref 7) |
| $Al_2O_3$ | 11373 steel | No | 7.2 | (Ref 7) |
| $Al_2O_3$ | 11373 steel | NiCr | 11.77 | (Ref 7) |
| $ZrO_2$+CaO | 35NiCr18 | NiCr | 24.5 | (Ref 102) |
| $ZrO_2$+CaO | 35NiCr18 | NiAl | 65.7 | (Ref 7) |
| $Al_2O_3$+2% $Cr_2O_3$ | 11373 steel | No | 8.37 | (Ref 7) |
| $Al_2O_3$+2% $Cr_2O_3$ | 11373 steel | NiCr | 8.97 | (Ref 7) |
| $Al_2O_3$+20% Al | 35NiCr18 | Al | 15.7 | (Ref 7) |
| $ZrO_2$+20% Al | 35NiCr18 | Al | 17.6 | (Ref 7) |
| $ZrO_2$+20% NiAl | 35NiCr18 | NiAl | 71.1 | (Ref 7) |
| $Al_2O_3$ | Steel | NA | 10.4 | (Ref 4) |
| $BaTiO_3$ | Steel | NA | 7.1 | (Ref 4) |
| WC | Steel | NA | 20.7 | (Ref 4) |
| $ZrO_2$ | Steel | NA | 10.3-11.0 | (Ref 4) |
| $ZrSiO_2$ | Steel | NA | 6.9-13.8 | (Ref 4) |
| $Al_2O_3$ | Stainless steel (Ra 0.6 μm) | NA | 32 | (Ref 102) |
| $Al_2O_3$ | Stainless steel (Ra 2.6 μm) | NA | 52 | (Ref 102) |
| $Al_2O_3$ | Carbon steel (Rz 18 μm) | NA | 33 | (Ref 103) |
| $Al_2O_3$ | Carbon steel (Rz 92 μm) | NA | 58 | (Ref 103) |
| $Cr_2O_3$ | Carbon steel | NA | 31 | (Ref 104) |
| $Cr_2O_3$ | CuZn alloy | NA | 20 | (Ref 105) |
| Hydroxyapatite (HA) | Ti6Al4V | NA | 49 | (Ref 106) |
| HA | Ti6Al4V | NA | 18 | (Ref 107) |
| $Al_2O_3$+13% $TiO_2$ | Al | NA | 27 | (Ref 104) |
| $Al_2O_3$+13% $TiO_2$ | Mild steel | NA | 16.8 | (Ref 108) |
| $ZrO_2$+8%$Y_2O_3$ | Carbon steel | NA | 34 | (Ref 109) |
| $ZrO_2$+8%$Y_2O_3$ | Carbon steel | NA | 18 | (Ref 109) |
| | (100 h exposure after sand blasting) | | | |

and condensates on the metal substrate surface. As a result, an oxide layer is formed on the substrate surface.

Generally, the oxide scale acts as an intermediate layer either to enhance or decrease the adhesive strength of the ceramic coatings. It was noticed that the adhesion of APS ceramic coatings (alumina) at 500°C much depends on the nature (compositions, structure) and morphology of the oxide scale. (Ref 1). For a stainless steel substrate, the preheating results in the formation of thin scales mainly consisting of a paramagnetic $Ni_xCr_yFe_{3-x-y}O_4$ spinel phase (polished surface) and an $Fe_{2-x}Cr_xO_3$ hexagonal phase (grit-blasted) (Ref 110). The thin oxide scale on stainless steel has a strong adhesion, even higher than 74 MPa for an Ni coating deposited on the preheated stainless steel to 650°C with a scale thickness of 288 nm (84 nm spinel at the top and 204 nm $Cr_2O_3$ beneath), with the fracture occurring from the interface between the coating and the glue (Ref 25). When alumina coatings are deposited at a deposition temperature higher than 300°C, the chemical bonding at the interface between the alumina splats and the oxide scale can be formed, being explained in detail later. Consequently, an adhesive strength of over 50 MPa higher than the strength of the adhesive glue can be achieved (Ref 111). It was reported that the initial oxide thickness

influences the adhesive strength of alumina coating on the blasted 316L deposited at ~500°C, i.e., an adhesive strength of 25 MPa as the minimum for a 17-nm-thick layer and 33 MPa for a 59-nm-thick scale (Ref 110). A thick oxide helps to achieve a high adhesion strength of the ceramic coating. The crystalline structure of the oxide scale may also affect the adhesion of ceramic coatings, being dependent on the matching degree of the crystalline constants of ceramic splats with the underlying oxide scale on the substrate (Ref 110, 112). An APS alumina coating deposited on a polished $\gamma$-$Al_2O_3$ surface at a deposition temperature of 600°C presented an adhesive strength of 35MPa, while, on a polished columnar $\alpha$-$Al_2O_3$ surface, it only became 3 MPa (Ref 113).

Since thermal spray ceramic coatings are generally adhered to a metallic substrate via surface oxide scale, the strength of the oxide scale significantly influences the adhesion, provided that the top of oxide scale is bonded well to the ceramic splat in the coating. Strongly adherent and dense oxide scale can contribute to the formation of strong bonding to ceramic coatings. With common plain carbon steel or low alloy steel, multiple oxide scales, mainly consisting of $Fe_2O_3$, $Fe_3O_4$, FeO with different amounts of alloy element solution, will form on the surface with different thicknesses, depending on the preheating history (Ref 114). The scale thickness may reach up to several 100 nm with a rough morphology (Ref 1, 97) by plasma jet heating. The rough thick scale surface not only results in splashed splats weakly adherent to substrate but also reduces the adhesion of the scale to the substrate. It has been revealed that scale layers with 173-nm-thick hematite at the top and 305-nm-thick magnetite beneath on a carbon steel substrate spalled upon the impact of molten $Al_2O_3$ spray droplets (Ref 1). On the other hand, Maitre et al. reported that, through pre-oxidation treatment in a controlled $CO_2$ atmosphere, a thick dense FeO scale of ~5 μm was formed (Ref 112). The alumina coating deposited on such a pre-oxidized polished steel presented an adhesive strength of 44 MPa, being comparable to that on the grit-blasted substrate while preheated by a plasma jet to a temperature of 400°C. This value is much higher than the 16 MPa with 20-μm-thick $Fe_2O_3$ and 28 MPa with 28-μm-thick $Fe_3O_4$. Since fractures occurred within the pre-oxidized oxides for all three samples, the strength of the oxide scale dominates the adhesive strength. With the polished steel substrate pre-oxidized to FeO when the scale thickness is less than 2 μm, the adhesive strength of the plasma-sprayed alumina coating increased with the decrease of scale thickness, and exceeded the strength of adhesive over 60 MPa with fractures in the adhesives (Ref 115, 116). Recently, Valette et al. achieved an unbelievable high adhesive strength of 105 MPa for the alumina coatings plasma-sprayed on a polished Ni substrate with a 1.8-μm-thick oxide (Ref 77). Such a high adhesive strength is related to the chemical bonding formation between the splat and the substrate oxide scale, and will be explained in the following section. Therefore, because the growing stress within the oxide scale increases with increasing oxide scale thickness, the scale thickness should be optimized according to its effect on the stress level and the thermal resistance to increase the splat–substrate interface temperature by lowering the heat sink effect. Thus, the control of both the thermodynamics and kinetics of substrate oxidation is essential to enhance the adhesion of the ceramic coating. Since the composition, crystalline structure, microstructure, and surface morphology of oxide scales much depend on the type of the substrate material, careful investigation of the oxide scale formation should be carried out when ceramic coatings are thermally sprayed in substrate preheated conditions.

## Intersplat Bonding Formation of Thermally Sprayed Ceramic Coatings

### General Features of the Microstructures and Intersplat Bonding of Thermally Sprayed Ceramic Coatings

It is well known that a thermally-sprayed ceramic coating usually presents a lamellar porous structure, especially when the coating is deposited mainly by sufficiently molten spray particles (Fig. 13). A certain porosity ranging from several percentages up to even over 40% is present in the coatings (Ref 2). Porosity creates poor coating cohesion to reduce wear and corrosion resistance. On the other hand, the coatings with a higher porosity are desirable for thermal barrier coatings (TBC) or abradable sealing (Ref 117), or

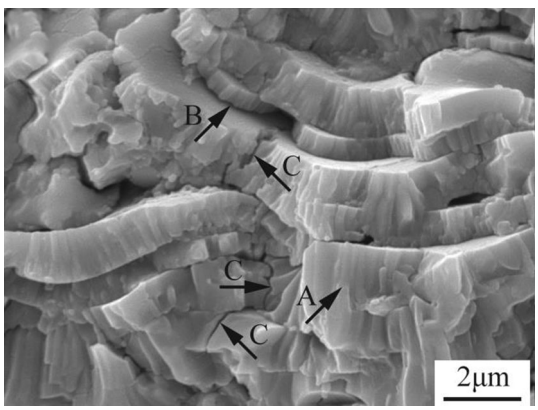


**Fig. 13** Typical features of plasma-sprayed ceramic coatings shown by a fractured cross-section of a YSZ coating. Arrows A, B and C indicate the bonded intersplat interface, unbonded splat interface, and intrasplat microcrack, respectively (Ref 40). Reprinted with permission from Elsevier

medical implant coatings (Ref 118). Coatings with a higher porosity of 30–70% can be fabricated by adding pore-formers into the spray powders (Ref 117) or using semi-molten spray particles (Ref 119). Three types of pores are present in a thermally sprayed ceramic coating. These include global pores, microcracks in individual splats, and unbonded splat interfaces. Global pores are formed by shadow effects and insufficient filling in cavities on the splat surface during molten droplet spreading, while microcracks form by quenching stress evolved during rapid cooling after splat solidification (Ref 98). The unbonded intersplat interfaces are considered as special two-dimensional pores with an opening of about 100 nm (Ref 120). All these pores affect the properties and performance of ceramic coatings.

Regarding the bonding formation in thermal spray coatings, early literature was mainly concerned with the adhesion of the coating to the substrate (Ref 4), possibly because the coating adhesion is much weaker than its cohesion (Ref 73). Moreover, in the 1960s and 1970s, rapid splat cooling and an amorphous formation became part of central research topics ,while thermal spray coating deposition via splat formation through molten droplet impacts fitted the topics well (Ref 71-73). As a result, the research on coating microstructures was more oriented to crystallite structures, such as quasi-stable phase formation, amorphous formation, and ultra-fine grain formation (Ref 72, 73, 121). Moreover, one of the major applications for refractory ceramic coatings is for TBC, and the requirements for low thermal conductivity with acceptable durability make the porous ceramic coating features be in the very nature of things (Ref 3). This is because the porous structures, especially with limited lamellar bonding in terms of real contact, attribute a low thermal conductivity to thermally-sprayed ceramic coatings. Therefore, due to the porous nature and the easy measurement of porosity in the coatings, the properties of the coatings were usually correlated with porosity following the empirical relationships for sintered porous ceramics. In a limited porosity range, the coating properties seemed reasonably correlated with porosity the same as that observed for sintered bulk (Ref 122). However, when the absolute property values were compared with the sintered bulk, the coating with the same level of porosity as that of the sintered bulk is much lower than that of the sintered bulk (Ref 11). This was attributed to the anisotropic features of the thermal spray coatings (Ref 123, 124).

McPherson and Shafer (Ref 9) first revealed the limited real contact between the lamellar interfaces by transmission electron microscopy (TEM). They also addressed the dominant effect of the limited real contact on the Young's modulus of plasma-sprayed ceramic coatings rather than their porosity. Through modeling the thermal contact resistance of lamellar-structured coatings using an ideal lamellar structure model, a relationship between the thermal conductivity and the real lamellar interface contact ratio was established (Ref 10). Based on the relative values of the Young's modulus of the alumina coating (Ref 9) and the thermal conductivity of $ZrO_2$ -based coatings (Ref 10), McPherson suggested that the real contact ratio between the lamellae was less than one-fifth to one-fourth in comparison with sintered dense bulk.

Taking advantage of the electrical insulation of plasma-sprayed alumina coatings, Arata et al. showed that all kinds of pores in the plasma-sprayed ceramic coating can be filled by metal through electroplating (Ref 125). Figure 14(a) illustrates a typical microstructure of a Cu-plated APS alumina coating taken by an optical microscope. Fortunately, the copper-plated $Al_2O_3$ coating presents an excellent contrast with $Al_2O_3$ itself under scanning electron microscopy (SEM) examination, and the unbonded interfaces have been visualized by the distribution of infiltrated Cu in the coating, as shown in Fig. 14(b, c) (Ref 126). Assisted by Cu as the tracer, it was found that the $Al_2O_3$ coatings plasma-sprayed at the spray distance from 80 mm to 200 mm present a similar lamellar structure (Ref 127, 128) (Fig. 15). Visually, it is clear to find that only limited splat interfaces are bonded to each other. By introducing the mean bonding ratio as the parameter (Ref 126, 129), the systematical characterization of the bonding ratio was carried out by tracking the splat interfaces in the coating delineated by the Cu distribution in Cu-plated $Al_2O_3$ coatings. The results showed that the bonding ratio increases with the increase of the plasma arc power, and rapidly reaches a saturated level of 32%. For the tracer, which is not visually seen under SEM examination, such as Cu-plated in YSZ coatings, Li et al. established an analytical method to estimate the mean bonding ratio through processing the energy dispersive x-ray line analyses of the data of the tracer (Ref 120). They proposed to infill the pores in the coating with certain oxides of the metal element excluded in the coating, through nitrate aqueous solution infiltration. Such a method can be applied to any coating material due to the availability of vast nitrates and their water-solubility. As shown in Fig. 16, both $Al_2O_3$ coatings (Ref 127) and YSZ coatings (Ref 130) deposited at a short spray distance present a high bonding ratio, while the bonding ratio begins to decrease when the spray distance is increased to a certain distance. For the $Al_2O_3$ coating, this distance is about 110 mm by also taking account of the fracture toughness change against spray distance (Ref 131), while for 8YSZ the distance is about 90 mm (Ref 130). Moreover, all these data reveal that the maximum bonding ratio is less than one-third. Those results are consistent with those predicted through the Young's modulus of the $Al_2O_3$ coating and the thermal

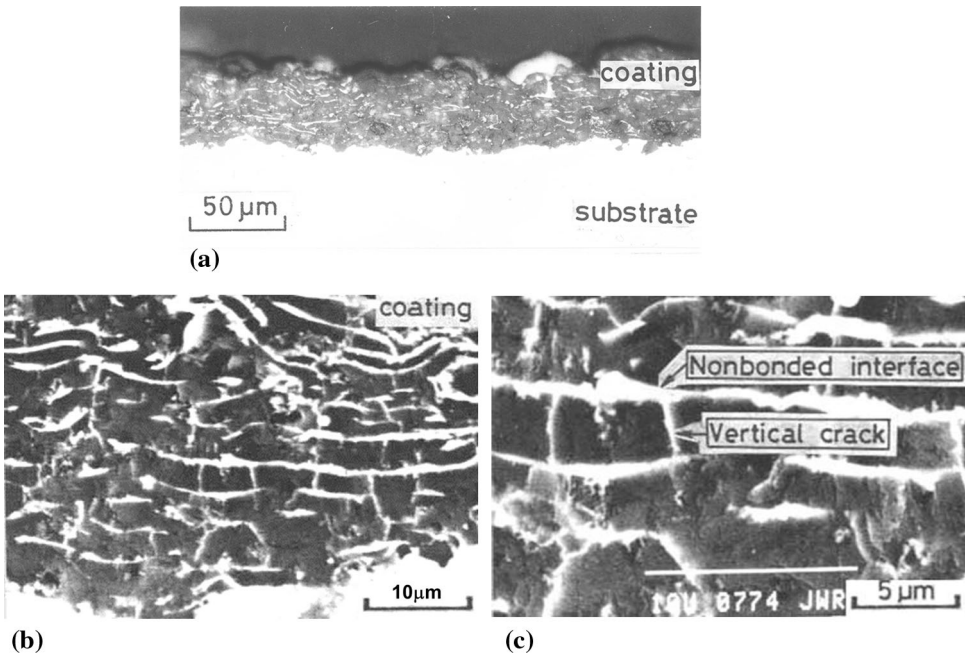


**Fig. 14** Typical pore networks represented by Cu distribution in a Cu-plated $Al_2O_3$ coating showing the large amount of the nonbonded splat interfaces and vertical intrasplat microcracks (white strings). (a) Microstructure by optical microscope; (b) and (c) SEM images at different magnifications (Ref 129). Reprinted with permission from Elsevier

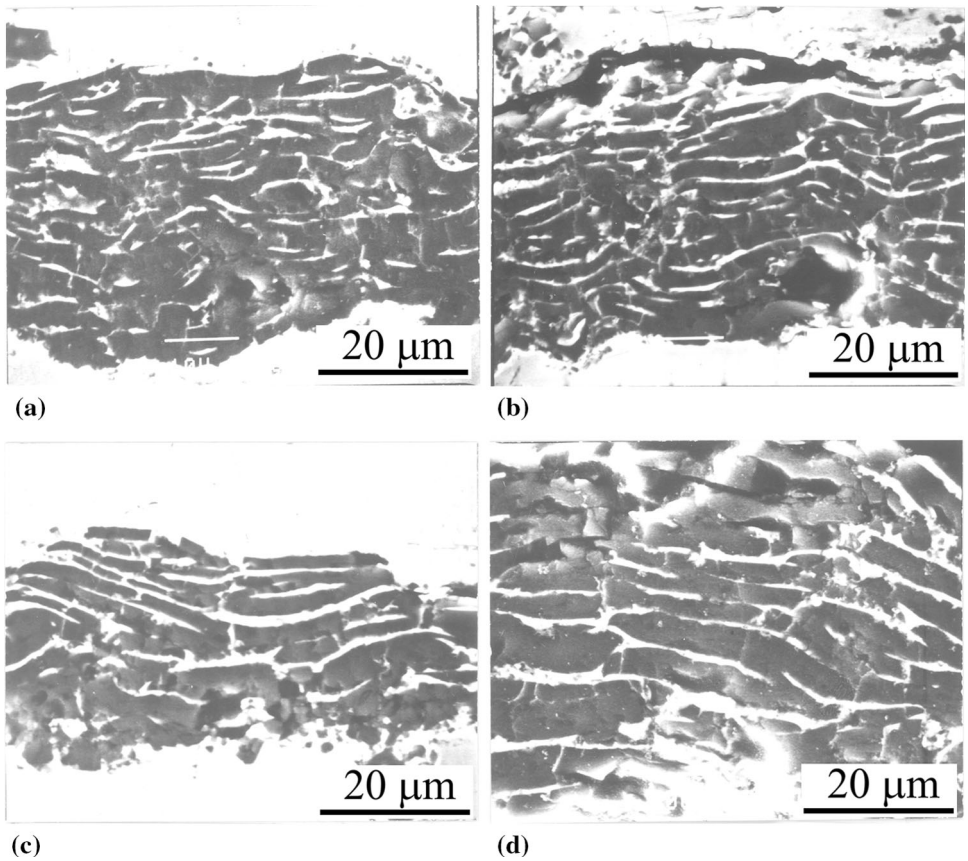


**Fig. 15** Cross-sectional images of plasma-sprayed $Al_2O_3$ coatings at different spray distances (a) 80 mm, (b) 100 mm, (c) 150 mm, (d) 200 mm, showing the similar lamellar structure with limited interface bonding revealed by the plated Cu distribution (white strings are copper plated into $Al_2O_3$ coatings). All coatings were deposited by one pass except for four passes at the spray distance of 200 mm. (Ref 127). Reprinted with permission from the Joining and Welding Research Institute of Japan

conductivity of the YSZ coatings by McPherson. As a conclusion, as visualized by the Cu-plated $Al_2O_3$ coating and estimations from the coating properties for YSZ, plasma-sprayed refractory ceramic coatings with a high melting point present limited intersplat bonding. The maximum bonding ratio is less than one-third. A more detailed review of the effect of spray parameters on the bonding ratio can be found in review papers (Ref 45).

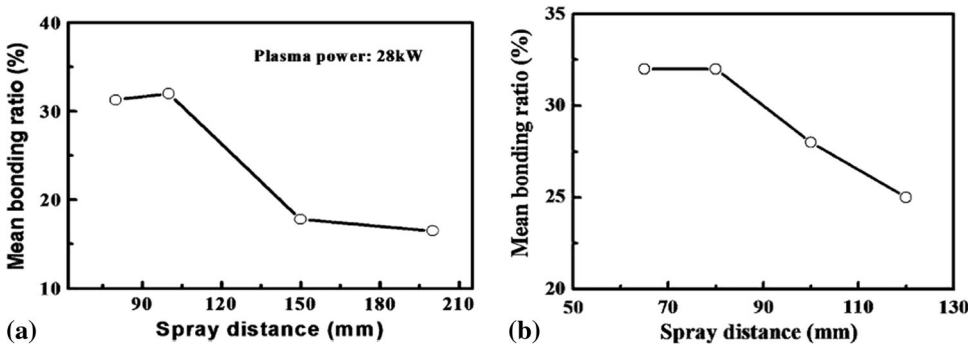


**Fig. 16** Effect of spray distance on the mean bonding ratio of a plasma-sprayed $Al_2O_3$ coating (a) (based on the data reported in Ref 127) and an 8YSZ coating (b) (based on the data reported in Ref 130)

## The Relationships between the Properties and Splat Bonding for Thermally-Sprayed Ceramic Coatings

Thermal spray coatings with lamellar structures exhibit a strong anisotropy of properties (Ref 123, 124). The properties, such as mechanical properties like Young's modulus, tensile strength, fracture toughness, and transport properties like thermal conductivity and electrical conductivity, are usually measured in two different directions, i.e., parallel to the splat plane and perpendicular to the coating surface. In this section, to examine the effect of spray particle parameters on intersplat bonding formation, theoretical relationships will be presented. This is because only limited data of the intersplat bonding ratio can be found due to the difficulty of quantitative characterization. On the other hand, based on theoretical relationships, the change of the bonding ratio within the coating can be examined through the change of coating properties.

The establishment of the property–structure relationship is primarily carried out using a brick-wall-like ideal structure model (Ref 10, 132). The coating consists of many identical layers with the same thickness (i.e., splat thickness, δ). Between each adjacent layer, only a fraction of the interface is chemically bonded, while the other interface areas are left as unbonded, with an opening of ~100 nm as two-dimensional pores. This bonded fraction is defined as the bonding ratio (α). The individual bonded interface areas are uniformly distributed at the interface. The diameter of a bonded area is a. The microcracks within each splat are not taken into account.

The first attempt to establish the relationship between the thermal conductivity and structural parameters was made by McPherson, utilizing the thermal contact resistance concept (Ref 10). Based on such an approach, the following relationship is obtained by only considering the heat conduction while neglecting the thermal radiation and convection within the pores (Ref 133):

$$\frac{\lambda_c}{\lambda} = \frac{2\delta\alpha}{\alpha\pi}\left(1 + \frac{2\delta\alpha}{\alpha\pi}\right)^{-1} \quad \text{(Eq 5)}$$

where $\lambda_c$ is the apparent thermal conductivity of the coating in the direction perpendicular to the coating surface, and λ is the thermal conductivity of the splat material itself. By neglecting the second term in the denominator, the above relationship is reduced to the one that was established by McPherson as follows (Ref 10):

$$\frac{\lambda_c}{\lambda} = \frac{2\delta\alpha}{\alpha\pi} \quad \text{(Eq 6)}$$

The above relationship is valid when the diameter of the bonded area is larger than the splat thickness. Accordingly, the thermal conductivity through the coating thickness is proportional to the intersplat bonding ratio. Since the contact resistance was originally introduced to estimate the contact area by testing the electrical conductivity, the above relationships are also valid for the electrical conductivity of thermal spray coatings. When the bonding ratio is larger than 39.2%, the effect of contact resistance in the bonded interface region can be neglected. Then, the electrical conductivity ($\sigma_c$) is directly proportional to the electrical conductivity of the splat (σ) as follows (Ref 134):

$$\frac{\sigma_c}{\sigma} = \alpha \quad \text{(Eq 7)}$$

The ratio of the Young's modulus of the coating ($E_c$) to that of the splat material ($E$) in the direction perpendicular to the coating plane is expressed as follows (Ref 132):

$$\frac{E_c}{E} = \alpha\left[1 + 2\pi\left(\frac{\alpha}{\delta}\right)^4 \beta^2 f(\beta)\right]^{-1} \quad \text{(Eq 8)}$$

where $\beta = \sqrt{\pi/8\alpha}$ and f(β) is a function of β, namely, a function of the interface bonding ratio. When α is larger than 40%, the second term in the denominator can be neglected. That is:

$$\frac{E_c}{E} = \alpha \quad \text{(Eq 9)}$$

Thus, Young's modulus is also proportional to the intersplat bonding ratio.

When the crack in a brittle ceramic coating propagates along the lamellar interface direction, the critical strain energy release rate as the fracture toughness $G_{IC}$ can be expressed as (Ref 131):

$$G_{IC} = 2C_P\gamma_e\alpha \quad \text{(Eq 10)}$$

where $\gamma_e$ is the effective surface energy of the splat material and $C_p$ is constant larger than one to modify the tortuosity of cracking passes.

When thermal spray coatings are subjected to solid particle impact, the impact-induced stress wave propagates through the coating. The interaction of the reflection of the wave at the unbonded interface with the transmission wave crossing the bonded interface causes tensile stress at the corner of the unbonded region. As a result, the unbonded interface region acts as pre-cracks and propagates through a bonded interface, leading to debonding and delamination of the splats. Accordingly, the erosion rate of brittle coatings at 90° impact excluding the cutting effect is determined by splat interface bonding. Supposing that the fraction of incident erosive particle energy for driving crack propagation is constant, the erosion rate can be related to the coating structure parameters as follows (Ref 135):

$$A_c = \frac{2\gamma_e\alpha}{KE_m\delta} \quad \text{(Eq 11)}$$

where $E_m$ is the mean kinetic energy of incident erosive particles and $K$ is a constant corresponding to the fraction of $E_m$ driving cracks to propagate.

The agreements between the results observed experimentally and those calculated by the theoretical equations are well recognized. As for a typical comparison of coating properties with the bulk counterpart, Table 2 shows the reported thermal conductivities of APS 8YSZ coatings. It can be found that thermal conductivity in a range of 0.8-1.3 W $m^{-1}$ $K^{-1}$ at room temperature was reported for 7-8YSZ deposited by different powders and processing conditions (Ref 136-148). Taking account of the thermal conductivity of 2.5-3 W $m^{-1}$ $K^{-1}$ for 8YSZ bulk (Ref 141, 149), the data reported above for the 8YSZ coatings are about one-third of the bulk YSZ. Such data are well explained by a lamellar structure with limited intersplat bonding. More detailed comparisons can be found in (Ref 11). Therefore, all the above theoretical equations can be used to reasonably estimate coating properties.

**Table 2** Thermal conductivity of plasma-sprayed 7-8YSZ coatings

| λc, W $m^{-1}$ $K^{-1}$ | References |
|---|---|
| 0.8-1 | (Ref 138) |
| 1.0 | (Ref 139) |
| 0.9-1.3 | (Ref 140) |
| 1.05-1.19 | (Ref 141) |
| 0.82-1.12 | (Ref 142) |
| 1.3 | (Ref 143) |
| 0.9-1.3 | (Ref 144) |
| 0.66 | (Ref 145) |
| 1.0 | (Ref 146) |
| 0.8-1.0 | (Ref 147) |
| 0.8-1.0 | (Ref 148) |
| 1.2 | (Ref 149) |
| 1.0 | (Ref 150) |

## Effect of Spray Molten Droplet Parameters on Intersplat Bonding Formation in Thermal Spray Ceramic Coatings

Nowadays, ceramic coatings are mainly deposited by plasma spraying. They can also be deposited by flame spraying using powders and rods, and the detonation-gun (D-gun) process, especially before the popular use of plasma spraying in the later 1950s. The main differences between those processes lie in the differences in the melting degree, temperature, and velocity of the spray particles as well particle size. Among all those spray methods, the spray particles generated by APS acquire the highest temperature, followed by Rokide flame spraying, HVOF, and the D-gun. While the D-gun-sprayed particles have the highest velocity, followed by HVOF, low-pressure plasma spraying (LPPS), and APS, then Rokide flame spraying (Table 3) (Ref 29, 27, 151-155). Moreover, the flame jet heating of the substrate or coating surface inevitably occurs during deposition, which depends on the traverse speed of flame jet to a substrate, and also influences the deposition characteristics. In this section, the effect of particle velocity and temperature on the bonding formation of ceramic coatings will be examined.

With the increase of the spray particle temperature, the deposition efficiency of the spray materials increases (Ref 86, 87). This means that the increased particle temperature promotes the cohesion formation for more spray particles. As shown in the previous section, the mean bonding ratio increases with the decrease of spray distance for both alumina and YSZ coatings. This change is reasonably consistent with the droplet temperature change against the spray distance, because the measurement showed that the temperature of ceramic spray particles decreases with the

**Table 3** Velocity data obtained for $Al_2O_3$ particles by different thermal spray methods

| Process | Particle velocity, m/s | References |
|---|---|---|
| APS | 150–250 | (Ref 152, 154-157) |
| LPPS | 300–400 | (Ref 27, 151, 152) |
| HVOF | 560–870 | (Ref 154) |
| D-gun | 600–1100 | (Ref 28, 153) |
| Rokide flame | 150–200 | (Ref 155) |

increase of spray distance from 50 mm (Ref 150). With the increase of the plasma arc power, it was also found that the mean bonding ratio is increased in a low power level range (Ref 127). However, when the increase of the power can ensure the sufficient melting of most spray particles, the mean bonding ratio reaches a certain saturated level, as recognized as 32-35% for hypersonic plasma-sprayed alumina (Ref 45). This fact has been well explained by the contradiction of particle heating and accelerating, because any effort to increase particle temperature by raising the plasma arc power tends to increase the velocity of the plasma jet. As a result, the heating time is decreased at a given spraying distance. The measurement of spray particle temperature revealed that increasing the plasma arc power mainly contributes to an increase in the numbers of spray particles that reach the full molten state (Ref 156, 157). Thus, the enhanced heating ability mainly compensates for the reduced heating time in high-temperature plasma jets, resulting from velocity increment. Moreover, with the temperature increase of the spray particles, their flattening degrees increase. Since the size of the splat central region where the dynamic transient pressure effectively acts on is limited to less than $\xi < 2$, the bonding forms more easily (Ref 84), and the enlarged splat size increases the splat interface area without effective dynamic pressure (Ref 158). This fact may limit the increase of the bonding ratio. Moreover, the reduced splat thickness by increasing the droplet temperature results in the decrease of the interface temperature because of the higher cooling rate.

On the other hand, it was widely believed that the increase of spray particle velocity tended to enhance the cohesion in the coating. This is because early investigations showed that the D-gun alumina coating presented a denser microstructure than the plasma-sprayed one. Moreover, the abrasive wear performance of D-gun coatings is superior compared with the plasma-sprayed counterparts (Ref 12, 159, 160). Moreover, a high impact velocity results in a high dynamic contact pressure, which enhances the infiltration of the spreading melt into surface cavities upon impact. However, when a D-gun alumina coating was subjected to Cu electroplating to reveal the intersplat bonding quality, as shown in Fig. 17, it was observed that the intersplat bonding of the D-gun alumina coating is very poor compared with that of plasma-sprayed coatings (Ref 161). This quantitative characterization yielded a mean bonding ratio of less than 10%. The examination into the crystalline structure of D-gun alumina presented a high fraction of $\alpha$-$Al_2O_3$ in the coating, which is the same as that of the feedstock powder, indicating that the spray particles are in a semi-molten state (Ref 162). Table 3 illustrates typical particle velocity data reported for different methods. Moreover, a 26 % mean bonding ratio was obtained

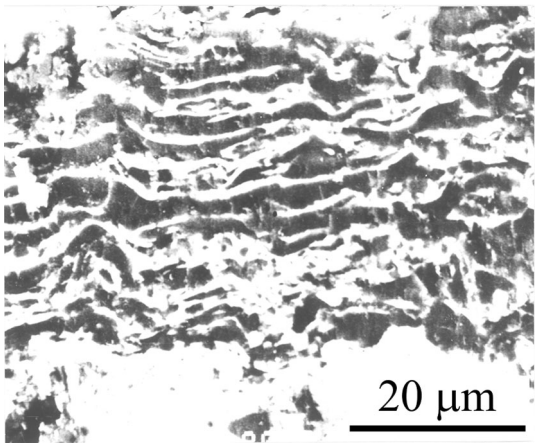


**Fig. 17** Microstructure of Cu-plated D-gun $Al_2O_3$ coatings showing the distribution of the unbonded interface regions by Cu (white strings) (Ref 161). Reprinted with permission from Elsevier

for low-pressure plasma-sprayed alumina coatings with a particle velocity between the APS and the D-gun (Ref 163).

The limited bonding ratio data for APS, LPPS, and D-gun $Al_2O_3$ coatings indicate that the interlamellar bonding ratio does not increase with the spray particle velocity. On the contrary, the mean bonding ratio decreases with the increase of spray particle velocity. This result can be attributed to the fact that the melting degree and temperature of spray particles decrease with the increase of their velocity (Ref 164, 165). The high amount of the $\alpha$-$Al_2O_3$ phase in the D-gun $Al_2O_3$ coating shows limited melting of the spray particles (Ref 162). A thermal conductivity of 2.08 W/(m K) was reported for D-gun alumina at $\sim$100°C (Ref 4). An HVOF alumina coating gave a thermal conductivity of 3-4 W/(m K) (Ref 154, 166). All those data are lower than the 4.75-5.1 W/(m K) which was reported for APS alumina (Ref 29, 152, 168). Based on the relationship between thermal conductivity and the bonding ratio (Ref 10, 136), all these data reflect a decreasing trend of the bonding ratio of alumina coatings in a sequence of APS, HVOF, and D-gun. The thermal conductivity of $Al_2O_3$ coatings increase with the spray particle temperature (Ref 136, 155, 167, 169). The comparison shows that the fracture toughness of HVOF alumina coatings is about two-thirds that of the APS coating (Ref 170). Since crack propagation along the splat plane is sensitive to effective intersplat bonding, a higher fracture toughness reflects a higher intersplat bonding ratio (Ref 131). Moreover, the ratio of fracture toughness of Rokide flame $Al_2O_3$ to ASP $Al_2O_3$ reported (Ref 155) is comparable to that of the thermal conductivity of Rokide flame $Al_2O_3$ to APS $Al_2O_3$ (Ref 169). Thus, the trends obtained for thermal conductivity and fracture toughness are consistent with the observed mean bonding ratio. Therefore, taking account of the spray particle velocity data shown in Table 3, it is clear

that greatly increasing the spray particle velocity by changing the spray method does not make any contribution to the intersplat bonding formation. On the contrary, the multiplication increases of spray particle velocity from APS to LSSP, then to HVOF and D-gun, leading to a significant decrease of intersplat bonding, i.e., real contact between adjacent splats. This fact reveals a completely different understanding from that of high velocity particle impact resulting in the formation of a dense and well-coherent coating. However, the question arises of how to explain the higher mechanical properties and mechanical performance of D-gun alumina coatings compared with plasma-sprayed ones.

The examination into the surface morphology of D-gun alumina coatings reveals a significantly different feature from APS coatings, as shown in Fig. 18(a) and (b) (Ref 161) Although its formation mechanism was not examined in detail, the D-gun coating presents a much rougher surface (i.e., splat surface) morphology in a micrometer scale, while APS alumina exhibits numerous smooth regions, as shown in Fig. 18(c) and (d) resulting from flattening of sufficiently molten particles. Such rough surface features can also be recognized in other D-gun coatings, such as the WC-Co reported by Tucker et al. (Ref 171). These surface features may be inherent in the high-velocity spray process and formed by semi-molten particles, although further investigation is required.

When the splat liquid does not wet the substrate enough due to either low wettability, low interface temperature, or a very short time, the infiltration of the melt into the cavities on the coating surface depends on the contact dynamic pressure. The size of the pore ($D$) into which the liquid will penetrate is given by (Ref 172):

$$D = -\frac{4\sigma \cos\theta}{P} \qquad \text{(Eq 12)}$$

where $\sigma$ is the surface tension of the liquid splat, $P$ is the effective dynamic pressure, and $\theta$ is the contact angle between the liquid and solid.

For $Al_2O_3$, taking $\sigma = 0.68$ N/m and $\theta = 180°$ as reported by McPherson (Ref 173), taking $P = 2.35\ \rho V2$ and $V = 150$ m/s, the typical size of the pores entered by the liquid of impact is approximately 0.013 μm. Considering the peak pressure rapidly decreases at a magnitude of one order in $10^{-8}$ s (Ref 26), the effective pore size entered by the liquid is approximately of an order of 0.1 μm. This value is coincidently consistent with the spacing between the unbonded splat interfaces (Ref 120). When substituting $V = 600$ and 800 m/s, the above pore size is decreased to 8 and 4.5 nm, respectively. This means that the cavity filling ability is increased by a magnitude of two orders under HVOF or D-gun conditions.

The high velocity impact of spray particles in the D-gun process results in a high dynamic pressure and increases

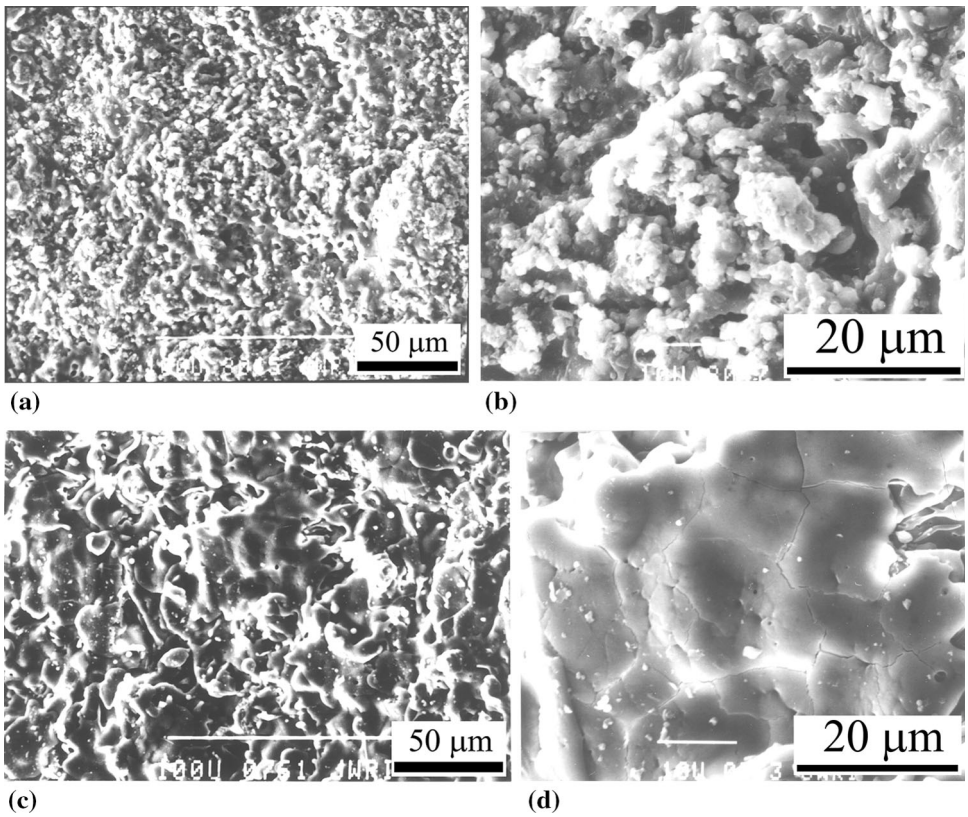


**Fig. 18** Comparison of typical surface morphology of a D-gun $Al_2O_3$ coating (a, b) with a plasma-sprayed $Al_2O_3$ coating (c, d) (Ref 161). Reprinted with permission from Elsevier

the cavity-filling ability of the molten melt. Moreover, the low temperature of the semi-molten particles restrains its flattening, which may make the dynamic pressure exert effectively in most of the splat interface. The high-velocity impact-induced shockwave interference may maintain the rough surface feature during splat deposition. The effective infiltration into the rough surface forms a strong interlocking effect. Such a mechanical interlocking effect could contribute to the high stiffness of the coating and high resistance to spalling of the splats under wear conditions. Therefore, it would be interesting in the future to examine the characteristics of such a rough surface, its evolution during coating build-up, and the formation mechanism to understand the mechanism of D-gun coatings presenting high mechanical performance.

### Effect of Substrate Surface Temperature on the Splat Bonding and the Concept of the Critical Bonding Temperature

Substrate surface temperature control is important in depositing ceramic coatings with the desirable properties, which includes preheating and cooling during spraying. It is known that the preheating of the substrate is a necessary process for thermal spraying of the coatings due to three reasons: (1) removing moisture or condensates from the substrate, (2) improving the adherence condition, and (3) accommodating the different thermal expansions between the substrate and the coating materials (Ref 1, 7). As mentioned previously on splat formation, the preheating temperature should be at least high enough to remove moisture to reduce the weakly adherent small particles by splashing and bubbles formed inside the splat. With a substrate surface prepared well, preheating to above 150 °C is required to ensure the removal of moisture from the substrate and direct contact of impacting molten particles with the substrate (Ref 1, 52).

The contact temperature between the spreading molten splat and the underlying substrate or deposited splats is positively related to the preheating temperature. The increase of the preheating temperature raises the contact temperature and enhances the possibility for chemical bonding formation at the interface upon molten droplet impact. Gyenis et al. showed that the adhesive strength of $Al_2O_3$ coating plasma-sprayed on a cast iron was increased to over 50 MPa at a preheating temperature of 180 °C from 10 to 14 MPa without preheating (Ref 111). When Funk et al. showed that, at a preheating temperature range from 60 to 240 °C for low carbon steel, bearing steel, and cast iron substrate, the adhesive strength of $Cr_2O_3$ coatings and $Al_2O_3$-40$TiO_2$ coatings was increased with increasing temperature (Ref 105). At a temperature over 100 °C, the fracture occurred substantially inside the coatings rather than at the coating/substrate interface. However, with Ni and brass substrates, the preheating showed no effect on the adhesive strength (Ref 105). With a 304 stainless steel substrate, when the preheating temperature was about 300 °C, the adhesive strength of $Al_2O_3$ coatings was increased to 34 MPa from about 15 MPa without preheating (Ref 110). As mentioned previously, the effect of preheating on the adhesive strength of thermal spray ceramic coatings much depends on the nature of the oxide scale formed on the metal substrate surface during preheating. Therefore, only a well-adherent dense oxide scale can effectively ensure high adhesive strength (Ref 77, 115, 116).

Many investigations have shown that, at an elevated preheating temperature, the intersplat bonding is effectively increased (Ref 30-42). To increase the strain tolerance of TBCs, Johner et al. proposed the depositing of thick YSZ coatings with segmented cracks through "hot spraying" to make each splat microwelded together (Ref 30). Through increasing the deposition temperature with preceding spraying, the splats became well bonded together, and referred to as microwelding at high temperatures. Gray et al. disclosed that the YSZ TBCs with a coherent, continuously columnar grain microstructure were deposited by increasing surface deposition temperatures higher than 600 °C (Ref 31). Heintze and Uematsu observed about 200-μm-long columnar grains in the top region of thick $Al_2O_3$ with α-phase when the coating was sprayed with APS, with a slow torch traversing to increase the deposition temperature with the preceding coating deposition (Ref 32). Similar effects were also reported by Jung et al. (Ref 33, 34). Therefore, with the increase of ceramic coating thickness, the rapid heat sink effect of the metal substrate disappears, and subsequently the temperature of coating samples can be significantly raised intentionally or unintentionally. All these facts reveal that enhanced intersplat bonding can be achieved by depositing ceramic coatings at an elevated deposition temperature. Accordingly, dense YSZ coatings with highly bonded splats deposited at high preheating temperature have been widely utilized to generate macrocracks perpendicular to the coating plane to enhance strain tolerance for highly durable TBCs in terms of dense vertically cracked (DVC) coatings (Ref 174). The effect of the deposition temperature on the splat bonding formation has been systematically investigated by gradually increasing the deposition temperature for YSZ (Ref 134) and $Al_2O_3$ coatings (Ref 43). By examining the fractured cross-sections of the coatings, the dependency of interlamellar bonding on the deposition temperature was qualitatively investigated. Based on the ionic conductivity measurement, it was quantitatively estimated that for YSZ coatings the apparent bonding ratio increases significantly with the preheating temperature to over 700 °C (Fig. 19) (Ref 134). Moreover, the examination into the

microstructure of YSZ coatings deposited at the preheated temperature of 810 °C reveals that the columnar grains usually observed in individual splats grow continuously to form larger columnar grains through the coating thickness (Fig. 20). This means that, at certain high preheating temperatures, the heterogeneous grain growth from the underlying splats during the spreading of spray molten droplets upon impact occurs with the suppression of uniform nucleation. As a result, the chemical bonding at the splat interface is formed through such heterogeneous grain nucleation and growth on the base of the grains in previous splats. The question here is at what temperature and why such heterogeneous grain growth occurs.

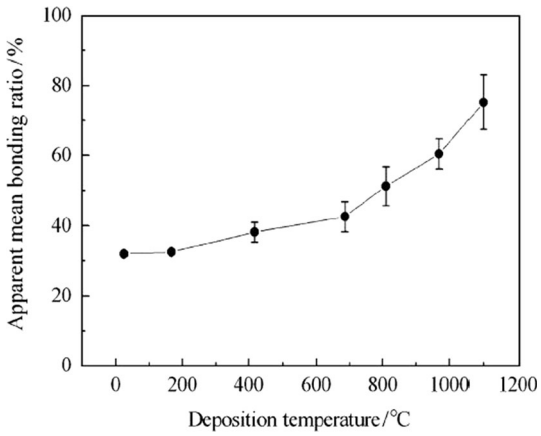


**Fig. 19** Effect of the deposition temperature on the apparent mean bonding ratio of a plasma-sprayed 8 mol% YSZ coating showing that the bonding ratio increases rapidly at a temperature higher than about 700 °C, corresponding to the critical bonding temperature (Ref 134). Reprinted with permission from John Wiley and Sons

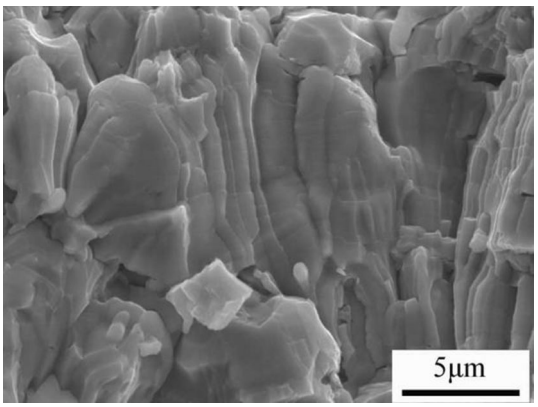


**Fig. 20** Typical morphology of a fractured YSZ coating deposited at the deposition temperature of 810 °C showing continuously grown columnar grains across the multiple splats indicating sufficient bonding at the splat interfaces (Ref 134). Reprinted with permission from John Wiley and Sons

Because the metal substrate oxidation occurs at the preheated conditions in ambient atmosphere, most investigations on the splat formation were mainly concerned with splat morphology and carried out at a narrow temperature range. Taking advantage of the fact that the deposition of oxide ceramic splats on an oxide ceramic substrate does not involve the effect of oxidation when plasma spraying is performed in an ambient atmosphere, the effect of preheating temperature on the interface bonding formation of ceramic splats were investigated in a wide temperature range to understand the dominant factors (Ref 43-45, 175-178). In all those tests, the substrate materials are the same ceramic material as the splat to experimentally simulate the intersplat interface bonding formation. Both the substrate temperature and droplet temperature determine the interface temperature between the spreading melt and the substrate. Since the heating of the plasma jet can provide additional thermal energy to alter the interface temperature, to eliminate the effect of plasma jet heating, a shielding plate with small holes of 1 mm diameter, permitting limited molten droplets to pass through to deposit isolated splats, was placed 20 mm ahead of the substrate. The fractured cross-sectional samples with splats deposited at different deposition temperatures were used to evaluate the interface bonding state at the first grade, since the coating fracturing tends to visualize the bonding through debonding the weakly bonded interface. It was found that at low deposition temperatures the fractured cross-sectional samples clearly show that the debonding occurs at the splat/substrate interface, which was recognized by the polished substrate surface flat profiles. Typical results are demonstrated in Fig. 21 for $TiO_2$ at 115 °C (Ref 44), $Al_2O_3$ at 270 °C (Ref 43), $La_2Zr_2O_7$ at 288 °C (Ref 175) and YSZ at 460 °C (Ref 43). At high deposition temperatures, the splats were bonded sufficiently to the substrate, as shown in Fig. 22 for $TiO_2$ at 200 °C, $Al_2O_3$ at 315 °C, LZO at 657 °C, and YSZ at 825 °C. By further reducing and refining the temperature increment to the transient temperature for the splat interface bonding change from the unbonding to the bonding, it was found that the transition temperature range from the unbonded to the bonded interfaces is rather narrow. For $Al_2O_3$ splats, as shown above, when the substrate preheating temperature, i.e, deposition temperature, is at 270 °C, no effective bonding was observed, while at the deposition temperature of 300 °C, the $Al_2O_3$ splat perfectly bonds to $Al_2O_3$ substrate as revealed by TEM of the cross-section (Ref 176). As a result, the critical deposition temperature for the cohesive bonding formation, in short the critical bonding temperature, was proposed (Ref 43). For $Al_2O_3$ and 8YSZ, the critical temperatures are 300 °C and 650 °C, respectively. A YSZ splat deposited on polycrystalline bulk YSZ at the deposition temperature of 700 °C was sampled by

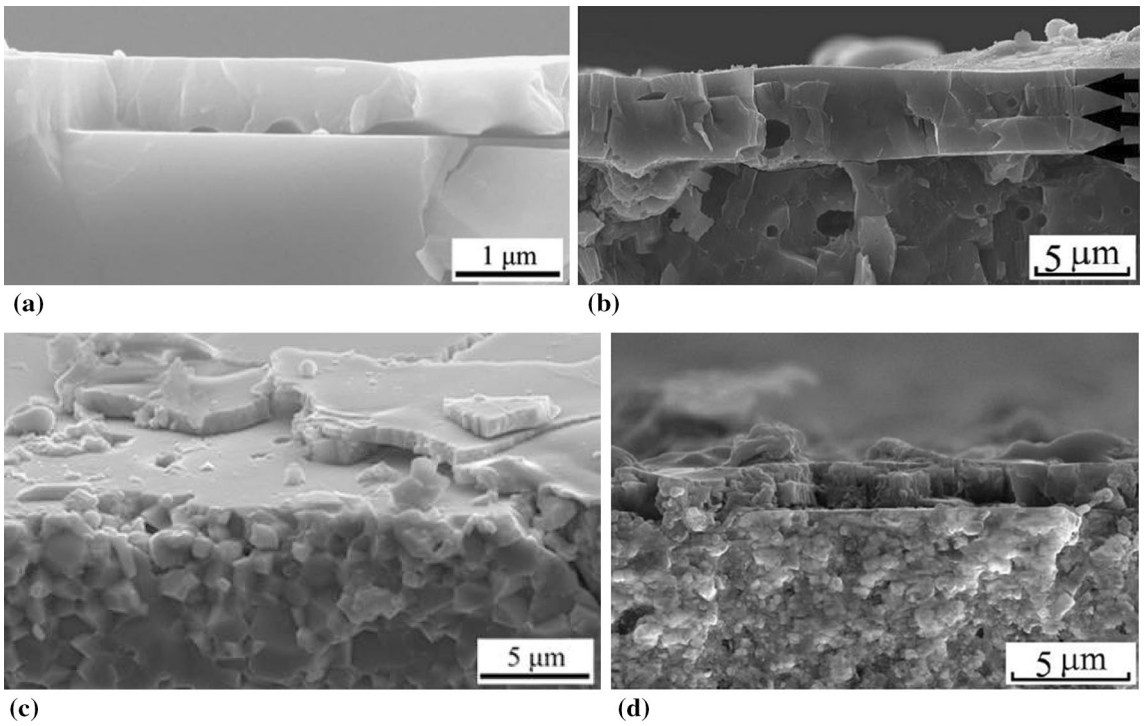


**Fig. 21** Typical cross-sectional morphology of fractured splats deposited by different materials on polished identical substrates at corresponding low deposition temperatures showing the interface delamination indicated without forming effective interface bonding. (a) $TiO_2$ at 115 °C (Ref 44) (Reprinted with permission from Elsevier); (b) $Al_2O_3$ at 270 °C (Ref 43) (Reprinted with permission from Elsevier); (c) $La_2Zr_2O_7$ at 400 °C; (d) YSZ at 460 °C (Ref 43)

focused ion beam and further examined by TEM (Ref 177). It was well confirmed that perfect bonding forms along all the interface. The microcracks in the splat deflect along the grain boundary when it runs to the splat/substrate interface. This also indicates a strong bonding feature. All the above splat depositions were made so that plasma spray conditions were optimized to acquire sufficiently molten spray particles with a temperature near their individual materials' melting points.

Systematical investigations on the critical bonding temperature of different oxide ceramic materials reveal that their critical bonding temperature is approximately linearly proportional to the melting point of spray ceramic materials (Fig. 23) (Ref 44). Therefore, to deposit a ceramic coating with a splat bonded chemically together, through heterogeneous grain growth from grains of previous splats underneath upon impact of molten spray particles, the surface temperature of the previous splats as the substrate here is required to be higher than the critical bonding temperature mentioned above for a given ceramic material corresponding to its melting point. Otherwise, the deposited splat remains unbonded to the underlying splats. This was confirmed through deposition of different ceramic coating materials (Ref 44)

The regression yields the relationship between the critical bonding temperature ($T_D$) and the melting point of the spray materials ($T_{m.p}$) as follows (Ref 178):

$$T_D = 0.58 \times T_{m.p.} - 890 \quad \text{(Eq 13)}$$

Following the above relationship, when the spray ceramic material has a melting point lower than 1550 °C, as long as the spray particles are fully molten, a dense coating with splats sufficiently bonded with each other can be deposited in an ambient atmosphere without substrate preheating. A recent investigation into the deposition of $K_2Ti_6O_{13}$ and $(Bi_2O_3)_{0.75}$ $(Y_2O_3)_{0.25}$ (YSB) having a melting point of about 1360 °C and lower than 1000 °C, respectively, showed that the plasma-sprayed $K_2Ti_6O_{13}$ (Ref 178) and YSB coatings (Ref 179) present a sintered bulk-like microstructure without any trace of the conventional lamellar structure. Figure 24(a) and (b) illustrates the morphology of the fractured cross-section and typical microstructure of a polished cross-section of a $K_2Ti_6O_{13}$ coating, respectively. The fractured surface showed little trace of a lamellar structure, and the polished cross-section illustrates the dense microstructure of the coating, although longitudinal microcracks may occur (Ref 178). The above results reveal that the lower the melting point of spray ceramic material, the lower its critical bonding temperature. Therefore, to deposit a dense ceramic coating having a

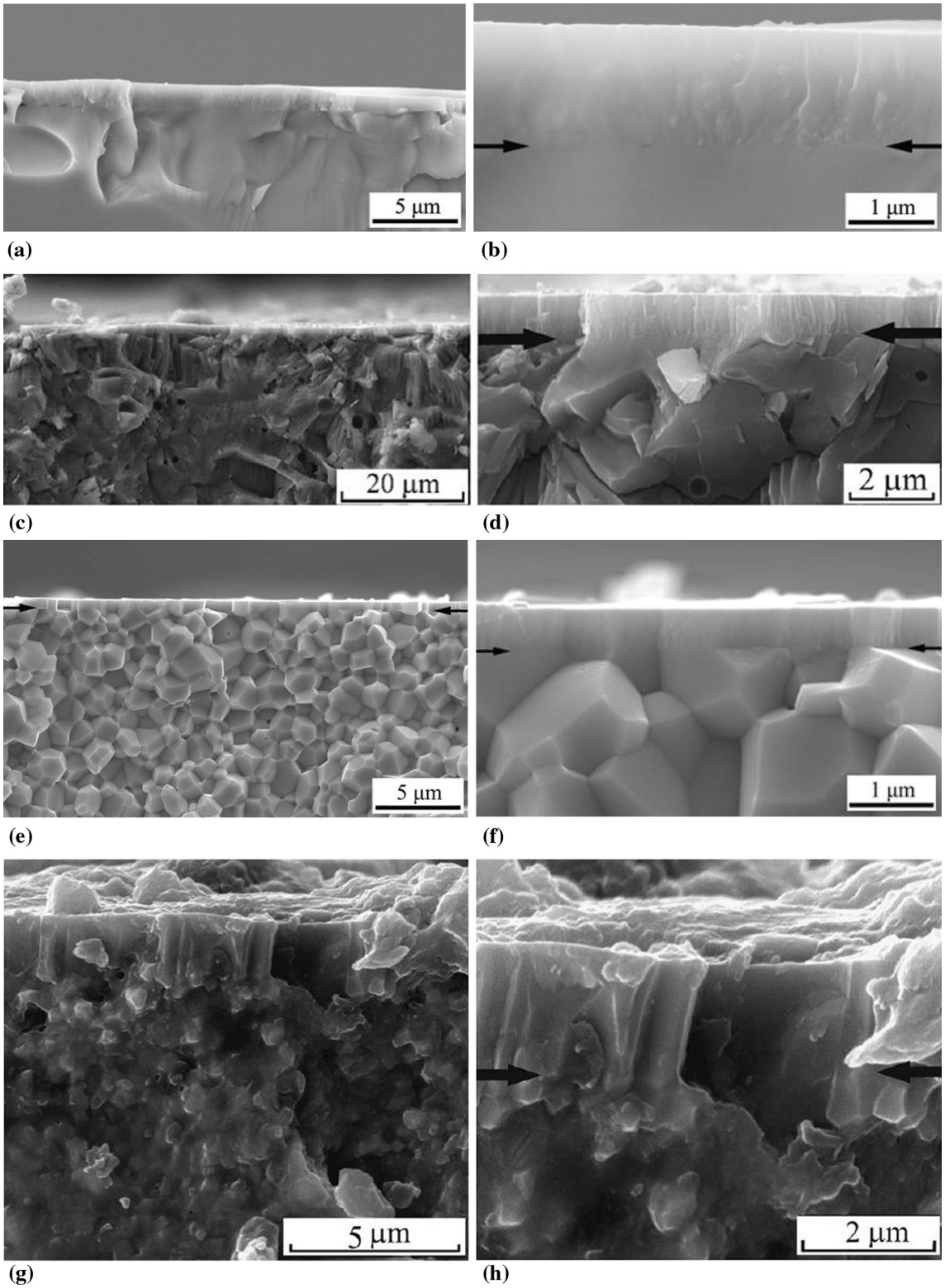


**Fig. 22** Typical cross-sectional morphology of fractured splats deposited by different materials on identical polished substrates at corresponding higher deposition temperatures than the critical bonding temperatures, showing a perfectly bonded interface without any evidence of debonding. (a) and (b) $TiO_2$ at 200 °C (Ref 44) (Reprinted with permission from Elsevier); (c) and (d) $Al_2O_3$ at 315 °C (Ref 43) (Reprinted with permission from Elsevier); (e) and (f) $La_2Zr_2O_7$ at 500 °C; (g) and (h) YSZ at 825 °C (Ref 43)

microstructure similar to sintered bulk, a lower preheating temperature is needed for low melting point material. Practically, for $Al_2O_3$-$TiO_2$ composite materials like $Al_2O_3$-13$TiO_2$ and $Al_2O_3$-40$TiO_2$, since their melting points are lower than that of $TiO_2$, the critical bonding temperature is less than 150 °C. This means that, if the normal preheating temperature for removing surface moisture can be maintained during the whole spraying process, sufficiently dense coatings can be deposited.

The concept of the critical bonding temperature proposed above defines the minimum deposition temperature condition necessary for molten ceramic droplets corresponding to their melting point temperature to form chemical bonding with the underlying ceramic splats during spreading after impact. That is, only when the deposition temperature is higher than the critical bonding temperature, can the impacting molten droplets form bonding with the substrate. Moreover, following the empirical equation, the critical bonding temperature for different ceramic materials can be estimated. Since the critical bonding temperature is related to the minimum interface temperature for bonding formation, a higher deposition temperature than the critical bonding temperature increases the interface temperature, and thus the activity of molecules involved in the bonding formation. Therefore, the bonding quality is improved with the increase of the deposition temperature. The microstructure and properties of thermally-sprayed ceramic coatings could be adjusted according to requirements by adjusting the deposition temperature.

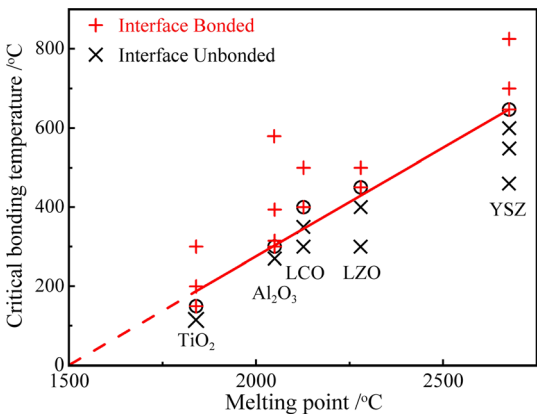


**Fig. 23** The relationship between the critical bonding temperature and the melting point of ceramic spray material (Ref 44). Reprinted with permission from Elsevier

The above critical bonding temperature theory can also be used to explain the achievement of the high adhesive strength of ceramic coatings deposited on metallic substrates. An examination of $Al_2O_3$ coatings with high adhesive strength reveals that all the coatings were coincidently deposited by keeping the deposition temperature higher than 300 °C, being the critical temperature for $Al_2O_3$ to form chemical bonding upon impact. Otherwise, the fracture during the tensile adhesive test occurs either partially or completely inside the coating. Valette et al. achieved an adhesive strength higher than 60 MPa for plasma-sprayed $Al_2O_3$ coatings even on a polished industrial carbon steel (Ref 116). More importantly, the coating was deposited at a preheating temperature of 400 °C. Although this deposition temperature was selected for completely desorbing adsorbates and condensates on the pre-oxidized surface, it is coincidently higher than the critical bonding temperature for $Al_2O_3$, which ensures a sufficiently higher cohesion throughout the coating than the strength of the glue used for the test. Moreover, chemical bonding also forms at the interface between the oxide scale and the alumina splats. When the preheating temperature is lower than the critical bonding temperature, partial fracture from the coating was observed due to the low cohesive strength.

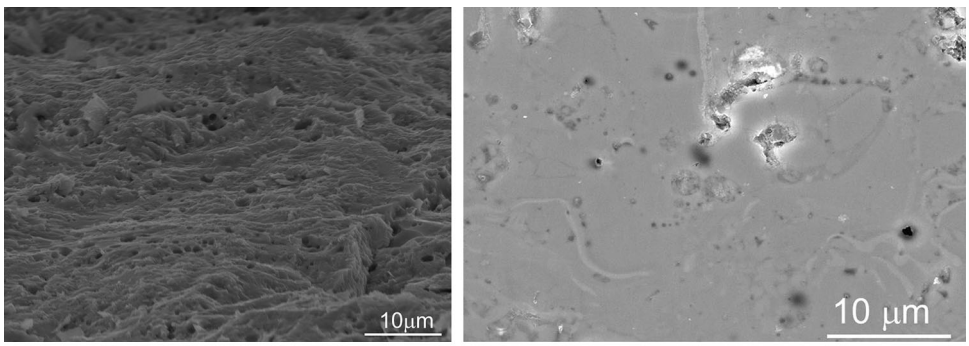


**Fig. 24** Morphology of the fractured cross-section of the $K_2Ti_6O_{13}$ coating plasma-sprayed at an ambient atmosphere without preheating, showing no any evident lamellar structure feature but a sintered bulk-like feature (a), indicating the formation of chemical bonding throughout the intersplat interfaces, and a typical microstructure of a polished cross-section of a $K_2Ti_6O_{13}$ coating (b) (Ref 178). Reprinted with permission from Springer Nature

## The Intersplat Bonding Formation Model and Mechanism

The formation of chemical bonding at the intersplat interface indicates that the atoms in the molten splats and the atoms in the substrate surface are sufficiently activated. This allows bond formation between the atoms across the splat interface in a very short time of a few microseconds when the deposition temperature is higher than the critical bonding temperature. A one-dimensional heat transfer model has been used to calculate the interface temperatures between the molten splat and the substrate for ceramic droplets at their melting points, and the deposition temperature corresponding to the corresponding critical bonding temperature, and Yao et al. found that the maximum interface temperature is approximately equal to the glass transition temperature, $T_g$ , for different coating materials (Fig. 25) (Ref 44). This result reveals that the bonding forms when the interface temperature is higher than $T_g$. Since the glass transition temperature is only determined by the nature of the spray material itself, it is defined as the intrinsic critical bonding temperature for a molten splat to form the chemical bond. As a result, an interface temperature larger than $T_g$ becomes the necessary and sufficient condition for impacting molten ceramic particles to bond with the underlying splats.

To understand the above conditions for bonding formation, it is necessary to understand the effect of supercooling on the viscosity and, subsequently, the activity of atoms in the supercooled melt. Splat formation during thermal spraying is a typical rapid cooling process. The solidification of the liquid splat takes place at a certain supercooling temperature, $\Delta T = (T_m - T)$, where $T$ is the temperature of the liquid splat and $T_m$ is the liquidus temperature of the splat material. To form chemical bonding for impacting molten splat, heterogeneous nucleation should occur from the grains on the previous splat surface. Heterogeneous crystal growth in glass-forming systems generally starts at $T \approx T_g$ and reaches a maximum at a temperature close to, yet beyond, $T_m$ (Ref 180). Due to the limited over-heating temperature of molten spray particles and rapid splat cooling, the solidification of liquid splat occurs at a temperature lower than its melting point, i.e., at supercooling. Figure 26 shows the relationship between the viscosity of different melts and their temperature ($T$) on $T_g/T$, reproduced from the reported data, being able to be expressed by a Vogel–Fulcher–Tammann empirical equation (Ref 181). In this figure, two data points for alumina at the temperatures of 2500 °C and its melting point 2050 °C were added in the original one in the literature to show the fragile feature of supercooled alumina melt. Based on the dependency of the viscosity on the temperature down to $T_g$, the melts are classified into two types: strong ones and fragile ones (Ref 182). For a strong melt like $SiO_2$, it has a very high viscosity of more than $10^5$ Pa s at the melting point, while a fragile melt like $A_2O_3$ has the much low viscosity of 0.05 Pa s at the melting point (Ref 183). The viscosity and relaxation times of strong liquids behave in nearly Arrhenius fashion, whereas fragile liquids show marked deviations from Arrhenius behavior (Ref 184, 185).

The viscosity represents the mobility and activity of the atoms in the melt. The mobility of atoms in molten melt decreases with the increase of the viscosity as the liquid temperature decreases towards $T_g$. There are two types of motion to provide the atoms with mobility for forming the bond, translational diffusion (slow relaxation α) and rotational diffusion (fast relaxation β) (Ref 184, 185). At higher temperatures, both the transactional and rotational

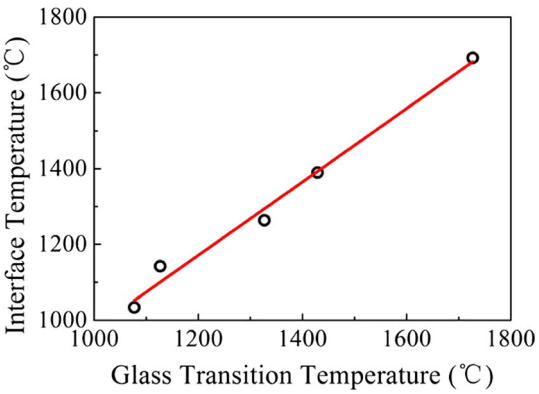


**Fig. 25** The relationship between the glass transition temperature and the maximum liquid splat–substrate interface temperature acquired by the impact of different ceramic droplets at their melting points on the identical substrate at room temperature

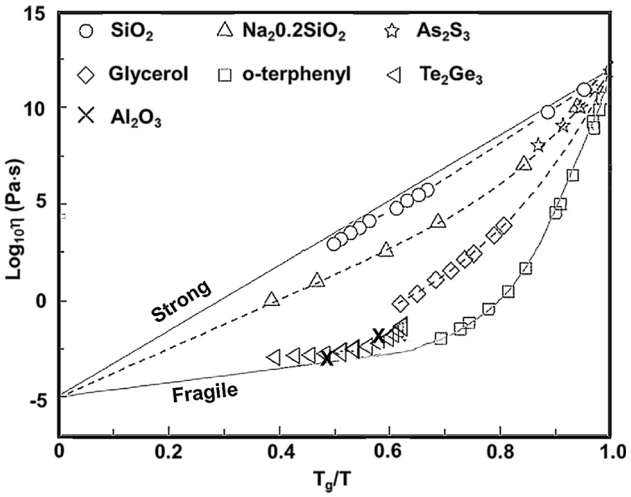


**Fig. 26** The relationship between liquid viscosity and $T_g$-based normalized temperature, showing the dependency of liquid viscosity on supercooling to $T_g$ for different glass-forming ability material liquids (replotted based on the data reported in Ref 184)

diffusion coefficients are inversely proportional to the viscosity, in agreement with the Stokes–Einstein and Debye equations, respectively. However, when the temperature is reduced to below about 1.2 $T_g$, the relationship between the transactional motion and viscosity breaks down. The transactional mobility rapidly decreases as the temperature decreases towards $T_g$ (Fig. 27) (Ref 184, 185). Finally, at $T_g$ , the transactional motion is frozen and molecules in the melt lose their mobility.

On the other hand, the properties of the supercooled liquid are related to the microstructure. It was conjectured and experimentally confirmed that the liquid contains many configurations (Ref 186, 187). Hu et al. found that, at high temperatures such as 2.5 $T_g$, the largest cluster has a volume containing only about 20 atoms (Ref 187). However, the cluster size drastically increases as the temperature decreases. As the temperature is below $T_g$, the largest cluster almost fills up the whole space. The percolation of the largest cluster can drastically slow down the dynamics for bonding formation because of its low atomic mobility. Rotall et al. also confirmed that the dynamic arrest is associated with the formation of a percolating network of locally favored structures, each in a local energy minimum and unable to reach the equilibrium state (Ref 188). Thus, the supercooling state is another factor controlling bonding

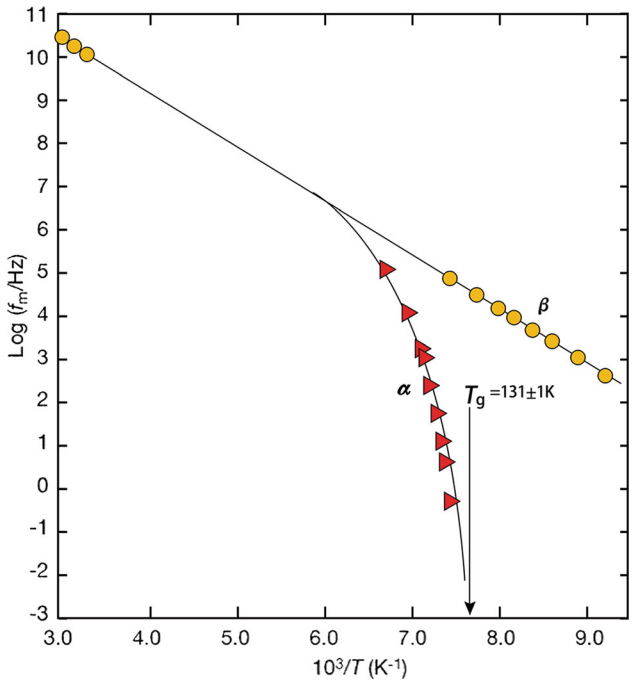


**Fig. 27** Using a mixture of chlorobenzene/cis-decalin (molar ratio 17.2/82.8%) as a glass-forming supercooled liquid for the temperature dependence of the peak dielectric relaxation frequency, showing the peak splits into slow (a) and fast (b) relaxations, corresponding to the transactional and rotational mobility of molecules in a moderately supercooled regime. The transactional motion is arrested at $T_g$ (Adapted from Ref 189)

formation. As the interface temperature becomes lower than $T_g$, the atoms in the melt are locally arrested in a large cluster.

From the point of view of thermodynamics, forming a chemical bonding interface, especially with a coherent boundary, will significantly decrease the interface Gibbs free energy. Thus, the bond formed over the interface should be a homogeneous reaction. However, due to the different microstructures between the supercooling liquid and the solid, the formation of chemical bonds requires atoms in the supercooling liquid to move to suitable sites on the surface, while the solid atoms can be regarded as fixed due to their low atomic mobility.

Based on the characteristics of the supercooled melt mentioned above and the intrinsic critical bonding temperature corresponding to the $T_g$ observed, Yao et al. proposed the bonding formation model shown in Fig. 28 (Ref 44). The interface between the spreading molten splat and the substrate (Fig. 28e) is unbonded immediately after they are brought into contact (Fig. 28d), due to the repulsive force across the interface (Fig. 28f). The atoms in the melt in contact with a solid surface for forming the bonding can be considered in the form of a cluster (Fig. 28b and c). At a temperature lower than *Tg*, the atoms in the cluster are tightly bound to each other and lose their transactional motion ability. They cannot move to the locations favored to form bonds with the atoms in the substrate (Fig. 28h). As a result, the chemical bonding does not form at the interface.

As the interface temperature becomes higher than *Tg*, the transactional motion of the atoms in the liquid splat recovers. Since most of the atoms in the supercooled liquid are still locally bound as quasi-clusters when the temperature is only a little higher than $T_g$, the interface bond can be formed prior to melt solidification, through a limited transactional local motion and rotations of the atoms in such clusters to local regions where the local structure is similar to the substrate (Fig. 28i). Consequently, the positioning of splat atoms in the form of quasi-clusters contributes to form bonds. As a result, the splat is even bonded to the solid surface via a liquid-like structure, i.e., an amorphous structure. As the liquid temperature is increased towards 1.05 $T_g$, the increased transactional motion also increases the crystal growth rate with an improved bond quality of nanocrystalline with fewer defects (Ref 189). On the other hand, at a sufficiently high temperature, as shown in Fig. 28(j), atoms with enough energy can completely break the bond with neighboring atoms in the cluster, rearrange, and migrate a longer distance to form bonds. Moreover, epitaxial grains grow across the splat interface (Ref 177, 190). Accordingly, even a coherent boundary can be formed between the splat and the substrate or previously deposited splats.

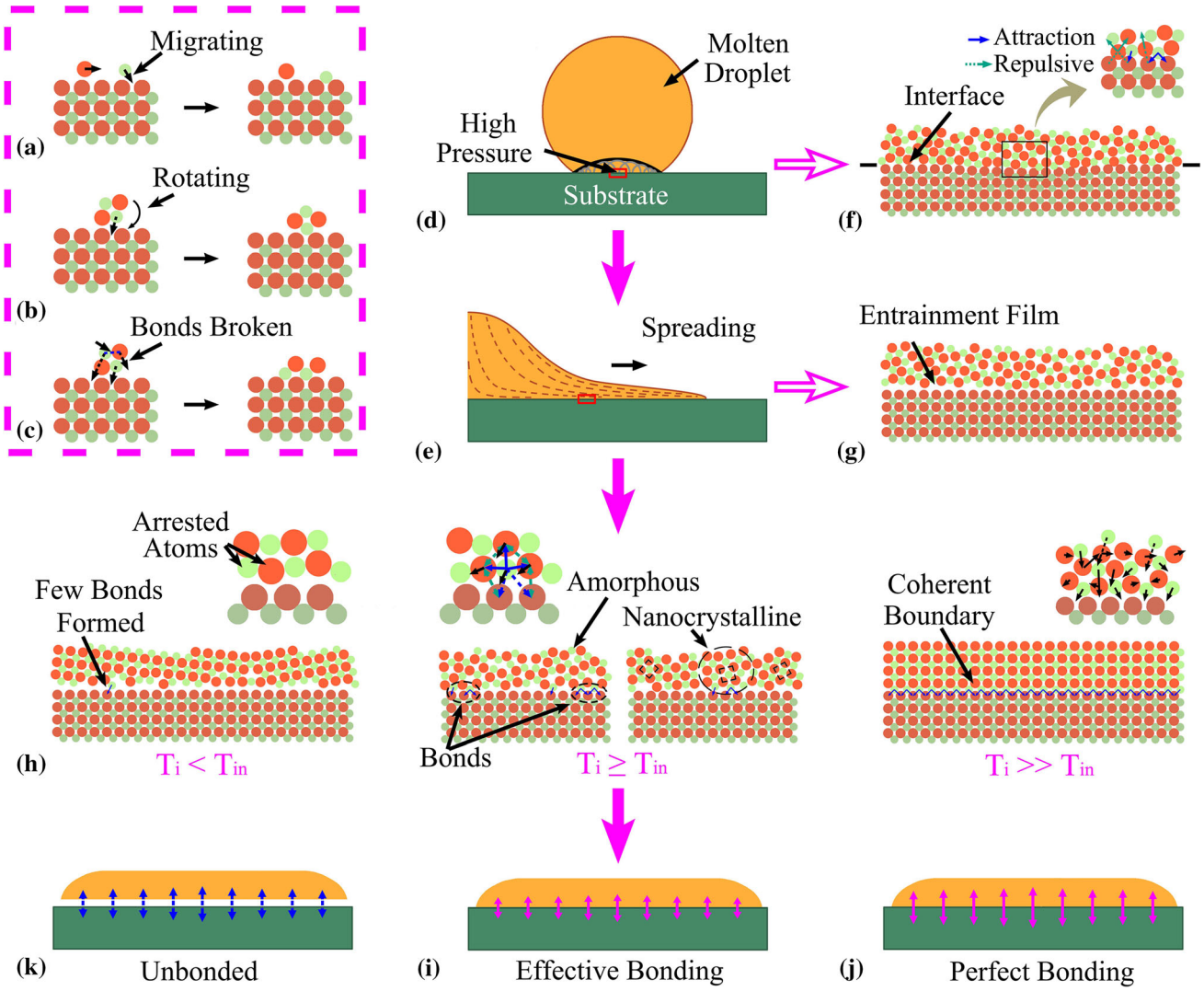


**Fig. 28** Model for impacting molten droplets to form bonding with the underlying substrate. (a–c) Possible motions of atoms in the melt for bond formation; (d, e) droplet impact and resultant flattening; (f, g) initial contact conditions; (h–j) the bonding formation corresponding to $T_i<T_g$, $T_i\geq T_g$ and $T_i>>T_g$; (k, i, j) the intersplat bonding states correspond to three different interface conditions: at $T_I<T_g$, the atoms in the liquid splat are arrested by the larger cluster and lose their activity for bonding formation; at $T_i>>T_g$, the atoms in liquid splat recover their activity to a limited level to just accommodate its positioning for bond formation with little change of the liquid structure; and at $T_i>>T_g$, the atoms break the bonds with other atoms in the liquid and form bonds with the atoms on the substrate by moving to the most favored position through epitaxial grain growth (Ref 44). Reprinted with permission from Elsevier

Based on the above model, the following important conclusions can be addressed:

(1) Only when the liquid splat–substrate interface in intimate contact reaches a temperature higher than $T_g$ can chemical bonding be formed at the interface between the impacting molten ceramic splat and the ceramic substrate underneath.

(2) At the interface temperature of a little higher than $T_g$, the solidified splat at the interface may contain an amorphous phase. This was observed in APS alumina (Ref 73, 176) and HVOF alumina (Ref 191), while a trace of amorphous phase near the interface in $TiO_2$ splat (Ref 44) and YSZ splat (Ref 192) reveals the initial amorphous phase, when taking account of the fact that the TEM examination process itself causes crystallization of the amorphous phase (Ref 191).

(3) The interface bonding quality changes with the interface temperature ($T_I$). Since the mobility of the atoms in the liquid splat increases rapidly with the increase of temperature at $T_I > T_g$, the increased transactional motion makes the atoms move to more suitable sites to form primary bonds with fewer defects. At higher deposition temperatures and subsequently higher interface temperatures, the

atoms in the melt have a high enough mobility to crystalline epitaxially, e.g., $TiO_2$ at 500 °C (Ref 190), $Al_2O_3$ at 800–900 °C (Ref 176), and 8YSZ at 1200 °C (Ref 177).

## Understanding the Limited Bonding Formation in Refractory Ceramic Coatings Based on the Critical Bonding Temperature Concept

Based on recent investigations into the conditions for intersplat bonding formation for thermal spray ceramics, two critical temperatures have been proposed: one is the deposition temperature, while the other is the interface temperature between the liquid splat and the underlying splat substrate. The latter in the critical condition is equal to $T_g$. Therefore, it is referred to as the intrinsic critical bonding temperature. For most ceramic materials, $T_g$ is equal to $\sim 2/3\ T_m$ (Ref 193). As a result, the intrinsic critical bonding temperature is well defined by ceramic materials.

The critical bonding temperature in terms of the critical deposition temperature is a processing parameter-dependent criterion. It is obtained by calculating the substrate surface temperature required to reach an interface temperature larger than $T_g$ through the impact of a spray molten droplet at its melting point. Among all the available thermal spray methods for ceramic coating deposition, plasma spray is the most effective for acquiring the highest spray particle temperature. Examinations into all the available data of ceramic spray particle temperatures reveal that in most cases there are a fraction of particles containing partially molten particles for high melting point ceramic spray materials. This is due to a wide range of size distribution of the practical spray powders, and subsequently the wide particle trajectory distribution in the plasma flame. Taking $Al_2O_3$ as a typical example, Zhang and Sampath showed that during plasma spraying the average surface temperature reaches 2500 °C and for most spray particles the melting index is less than one (Ref 194). This fact suggests that most spray particles contain an unmelted core despite the high surface temperature. Accordingly, only a fraction of molten particles lead to bonding formation with previous underlying splats upon impact. In this sense, this critical bonding temperature is of essential practical importance. As has been pointed out, the minimum substrate temperature required for intersplat bonding formation decreases with the increase of the sprayed molten particle temperature. The TEM analyses revealed that, at the deposition temperatures of 300 °C and 400 °C, a little higher than the critical bonding temperature, APS splats present an amorphous structure (Ref 177). The amorphous phase was also recognized at the interface vicinity near the bonded region in the APS alumina coating (Ref 196). The crystallization rapidly transforms to the nanocrystalline $\gamma$-$Al_2O_3$ phase with the grain growth. HVOF $Al_2O_3$ splat presents an amorphous phase (Ref 191). It should be pointed out that the crystalline structure in the splat is sensitive to local cooling conditions. For APS $Al_2O_3$ coatings, it was observed that the splat fraction over the unbonded interface presents the $\gamma$-$Al_2O_3$ phase due to the local high thermal contact resistance (Ref 196), and this is because the splats over the unbonded interfaces tend to solidify to crystalline rather than the amorphous phase due to the poor contact resulting in a reduced cooling rate.

Figure 29 presents the effect of substrate temperature and spray particle temperature on the interface temperature of the splat–substrate for $Al_2O_3$ of $T_g$ = 1177 °C. With the increase of the molten droplet temperature, the substrate temperature required to fulfill the intrinsic critical deposition temperature condition decreases. With the $Al_2O_3$ particle at 2454 °C, its impact on the alumina substrate at room temperature leads to bonding formation at the interface. Moreover, it should be pointed out that during one spray pass multiple layers of splats stack to form a coating. Some of these particles may impact on the hot splats whose temperature is locally higher than 300 °C. As a result, bonding forms at those local interface areas. Moreover, since the cooling rate and the interface temperature are inversely proportional to the square of the liquid splat thickness, the larger spray particles when fully molten benefit the formation of the bonding through the formation of a thick splat (Ref 195).

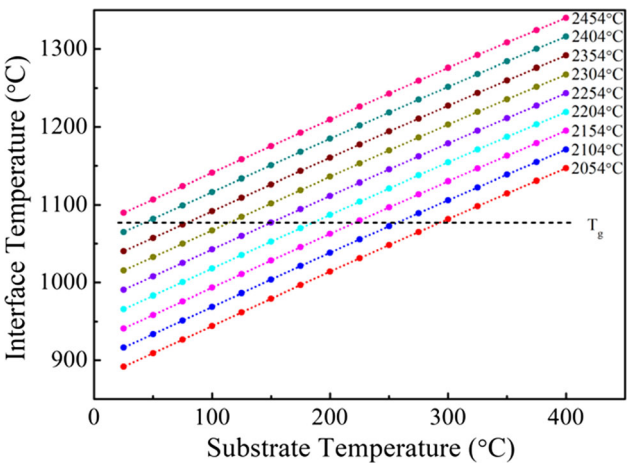


**Fig. 29** Effect of molten $Al_2O_3$ splat temperature and substrate temperature on the liquid splat–substrate interface temperature in comparison with the $T_g$ for 1-μm-thick liquid splat

### Strategy for Deposition of Dense Ceramic Coatings with High Performance Endowed by Sufficient Intersplat Bonding

As mentioned previously, the mechanical performance, including resistance to mechanical delamination or lamella spalling, wear, and transportation properties, such as thermal and electrical conductivity, depend on intersplat bonding. Therefore, the deposition of ceramic coatings at deposition temperatures higher than the critical bonding temperature benefits the full utilization of spray-coating material potentials.

The wear resistance of thermal spray ceramic coatings can be positively increased with the increase of intersplat bonding. During abrasion wear, the lamellae detachment resulting from limited splat bonding degrades the wear performance (Ref 197). Therefore, ceramic coatings with sufficiently bonded splats deposited at a deposition temperature higher than the critical temperature are expected to exhibit excellent wear performance. With erosion wear, as given by Eq 11, the erosion rate is inversely proportional to the mean bonding ratio. On the other hand, the erosion resistance, being expressed as the reciprocal of the erosion rate, is positively proportional to the splat bonding. This relationship has been confirmed experimentally (Ref 135). It is known that the maximum bonding ratio of a plasma-sprayed $Al_2O_3$ coating with optimized conditions at ambient atmosphere without preheating is less than one-third. Therefore, it is reasonable to consider that the coating deposited at a deposition temperature higher than 300 °C, being the critical bonding temperature, will present an enhanced wear resistance by a factor higher than at least three. Erosion tests have shown that the erosion rate of an $Al_2O_3$ coating deposited at 300 °C is less than one-third that for the counterpart deposited at room temperature (Ref 198). The observed results agree well with that expected theoretically. However, when YSZ coatings were plasma-sprayed at the preheated substrate temperatures of 75 °C and 300 °C, erosion tests yielded erosion rates of 0.92 mg/g and 0.79 mg/g, respectively (Ref 199). Only a very limited improvement by a factor of $\sim$10% was achieved. This can be reasonably attributed to little change of intersplat bonding (Ref 134), since all the YSZ coatings were deposited below the critical bonding temperature of 650 °C.

When $BaTiO_3$ was deposited at a temperature of 300 °C, being higher than the critical bonding temperature regarding its melting point, the coating exhibited sintered bulk fractured morphology showing well-bonded splats, and the deposits presented enhanced relative permitivity (Ref 200). For the ionical conductive electrolyte, $La_{0.8}Sr_{0.2}Ga_{0.8}Mg_{0.2}O_3$, the plasma spraying at a temperature higher than the critical bonding temperature yielded the electrolyte with over 80% ionic conductivity of sintered bulk, permitting the assembly of solid oxide fuel cells with high output performance (Ref 201).

A high-performance TBC not only requires a high thermal insulating effect through using a coating with a low intersplat bonding ratio and thus low thermal conductivity but also a high fracture toughness resulting from high intersplat bonding. These two requirements are contradictory for TBCs. The deposition of a coating with a high bonding ratio and thus high fracture toughness, acquired simply by controlling the deposition temperature, enables a double-layered TBC design with a high thermal cycling lifetime (Ref 202, 203). Therefore, based on the switching of the deposition temperature from lower to higher than the critical deposition temperature, it becomes possible for APS to deposit ceramic coatings with controlled lamellar bonding from limited bonding to sufficiently bonding to exhibit a high performance comparable to those of sintered bulk ceramics.

Since the liquid splat–substrate interface temperature is positively increased with the increase of both the substrate preheating temperature and the droplet temperature, as shown in Fig. 29, by increasing the molten spray particle temperature, a dense ceramic coating with fully bonded splats can be deposited at a low deposition temperature (Ref 204). Therefore, it is also possible to reduce the preheating substrate temperature requirement by raising the spray particle over-heat temperature, although the high molten droplet temperature tends to reduce the interface temperature by decreasing the splat thickness.

## Prospectives on Applications of the Bonding Formation Theory to Improve the Load-Bearing Ability of Ceramic Coating System

The coating–substrate interface is regarded to be the weakest interface, since, until very recently, the adhesion of a ceramic coating is mainly contributed by mechanical interlocking. The low adhesion limits the load-bearing ability. A high load-bearing ability depends on the simultaneous strengthening of all the interfaces in the coating system, including the metallic substrate–oxide scale interface, the oxide scale–coating splat interface, the splat–splat interface, and the oxide scale itself. When a careful pre-oxidation is carried out, such as by oxidation in a $CO_2$ atmosphere to grow epitaxial FeO for carbon steel, and to NiO for Ni with a proper thickness less than 2 μm, not only the substrate–oxide scale interface but also the scale itself are strengthened. In such a case, the adhesion/cohesion strength depends on the scale–splat adhesion and the plat–splat cohesion. For alumina, when the coating is deposited at a temperature higher than 300 °C on a thick scale,

bonding at the above-mentioned two interfaces forms. Thus, adhesion/cohesion strengths of up to 105 MPa for the Ni substrate (Ref 77) and higher than 62 MPa for the carbon steel (Ref 116) were obtained. For 304 stainless steel, deposition without any preheating yielded an adhesive strength of about 10 MPa. Since the cooling rate of liquid splats deposited on metal substrates can be one order higher than that deposited on ceramic substrates (Ref 48), the thickness of the pre-oxidized scale should be controlled to achieve an interface temperature higher than the intrinsic bonding temperature for the formation of chemical bonding between the oxidized substrate and the first layer of the splats.

Therefore, for a metallic substrate, through forming a dense and well-adherent oxide scale thick enough to reduce the cooling rate under well-controlled pre-oxidation conditions, a ceramic coating with a higher adhesion/cohesion strength exceeding 100 MPa can be deposited by depositing the ceramic coating at a temperature higher the critical bonding temperature. Accordingly, to achieve the ceramic coating system mentioned above, the understanding of the oxidation thermodynamics and kinetics for different kinds of metal substrates under a controlled oxidation atmosphere to grow a well-adherent, dense oxide scale with a controllable thickness is of essential importance. Moreover, the study also needs how to grow a conformal scale on a blasted substrate surface with a uniform thickness and without any sharp corner effects.

## Conclusions

Thermal spray coating formation involves two types of bonding, adhesion between the metallic substrate and the ceramic splats and cohesion between the ceramic splats. The adhesive strength primarily involves multiple heterogeneous interfaces: metal/oxide-scale/ceramic-splat/splat, while the cohesive strength only involves the homogeneous splat/splat interfaces. Since the adhesion and cohesion determine the successful applications of ceramic coatings and their performance, they are the central concerns accompanying the development of thermal spray technology. The main progress in understanding the bonding formation fundamentals can be summarized as follows.

(1) The splat formation characteristics determine the kinetics for the bonding formation after molten droplet impact. The bonding forms within 10 μs due to the rapid splat cooling. The time for the adhesive bonding is shorter than that for cohesive bonding formation due to the higher thermal effusivity of the metal substrate compared with oxide ceramic splats. The splashing-induced arms and small particles weakly adhered to the substrate decrease the adhesion, which needs further investigation in detail. The impact of molten droplets forms regular disk-shaped splats on a flat clean substrate with evaporative adsorbates or condensates removed by preheating, or without gas phase evolution at the interface. For simple physical absorption of moisture, a preheating temperature higher than 150 °C leads to the formation of disk-shaped splats on a flat substrate. Moreover, the transition temperature from irregular splat to regular disk shape can be influenced by chemisoption features of the substrate materials. Preheating promotes an intimate contact of the spreading melt with the substrate without any gas interference, resulting in excellent thermal contact at a resistance lower than $10^{-7}$–$10^{-8}$ K $m^2$/W, being favorite for bonding formation. The cooling rate of the spreading melt reaches an order of 400–800 K/μs which is increased by a factor larger than two when impacting on a metal substrate rather than ceramic substrate. The high contact pressure forcing spreading the melt to intimate contact with the substrate under high velocity impact acts only on the splat region less than the flattening ratio $<2$.

(2) The adhesion of thermally-sprayed ceramic coatings directly deposited on a blasted substrate at ambient atmosphere is dependent on the substrate roughness, and is usually less than 20 MPa. The introduction of a metallic bond coat can increase the apparent adhesive strength up to about 60 MPa. The apparent adhesive strength is also inevitably influenced by the features of the oxide scale on the substrate surface, including its chemistry, crystalline structure, morphology, and strength, and also the cohesion of the coating. Through pre-oxidation treatment of metallic substrates before spraying to form a dense oxide scale of a few micrometers thick on the substrate, an adhesive strength higher than 100 MPa can be achieved for alumina coatings deposited on a polished substrate along with deposition temperature control.

(3) Thermal spray ceramic coatings usually present a porous lamellar structure. The intersplat bonding within thermal spray refractory ceramic coatings is limited to less than one-third of the total interface area. The intersplat bonding states can be visualized by infiltrating the tracer into the gaps between the splats as the unbonded interface regions. The mean bonding ratio increases with the increase of the spray particle temperature and decreases with the increase of the spray particle velocity. The high spray particle velocity as observed for D-gun spraying enhances the coating wear performance, resulting from the

high infiltrating ability to spread melt in the rough surface cavities for enhanced mechanical bonding, although the effect of spray particle velocity on the splat surface morphology needs to be clarified.

(4) The theoretical relationships between lamellar structure parameters and several coating properties, including Young's modulus, fracture toughness, thermal conductivity, and electrical conductivity exhibit the dominant influence of the intersplat bonding on the coating properties. The limited maximum bonding ratio of less than one-third of those for the sintered bulk is responsible for the corresponding properties of the coatings less than one-third of sintered bulk of identical materials.

(5) The deposition at elevated high deposition temperatures promotes the columnar grains' continuous growth across multiple splats and chemical bonding formation at intersplat interfaces. Most importantly, recent studies have revealed that a liquid splat–substrate interface temperature higher than the glass transition temperature of the spray materials is a necessary and sufficient condition for impacting the splat to form chemical bonding with the underlying splats. The concept of the critical bonding temperature, i.e., the minimum substrate temperature for liquid splat to form chemical bonding upon impact, is proposed to be used for controlling the intersplat bonding formation. The critical bonding temperature of certain ceramic spray materials can be simply estimated by the linear relationship between the critical bonding temperature and the melting point of the spray materials. Thus, the condition for certain ceramic spray materials to form a bulk-like dense coating with the intersplat interface completely bonded becomes well understood. For ceramic materials with melting points lower than $\sim$1500 °C, the critical bonding temperature becomes less than room temperature. As a result, dense coatings with sufficiently bonded lamellae are deposited at room temperature.

(6) The model for impacting liquid splat to form bonding during spreading is proposed to explain the effect of the interface temperature on the bonding formation. As the liquid splat–substrate interface temperature becomes higher than but near the glass transition temperature, the activity of atoms in the melt just recovers to be able to move locally to favorite locations forming the bond with substrate atoms. If the interface temperature is lower than the glass transition temperature, no effective bonding forms at the interface due to arrest of the atoms' transactional motion. Thus, at a deposition temperature close to the critical bonding temperature, bonding is formed through the amorphous phase. The interface bonding quality is improved through heterogeneous grain growth of the grains on the substrate splats during solidification of the liquid splat to epitaxial growth with increasing deposition temperature. The fact that the bonding forms through the whole intersplat interface in a couple of microseconds reveals that thermal activation is mainly responsible for the chemical bonding formation regarding the negligible dynamic contact pressure in the region $\xi > 2$.

(7) For the adhesion of thermal spray ceramic coatings with the metallic substrate, the adhesive strength is determined by the weakest one among multiple interfaces and the scale itself, consisting of metal/oxide scale/splat/splat. If only the simultaneous strengthening of all the involved interfaces and the oxide scale on the substrate is realized, excellent adhesive strength can be achieved. Pre-oxidation of the substrate in a controlled atmosphere can form oxide scales grown from substrate grains with good matching of crystalline grains at the interfaces with excellent bonding and with a compact structure of high strength. Moreover, the interface between the oxide scale and the splats can be ensured through control of the deposition temperature higher than the critical bonding temperature. This has been well demonstrated by APS $Al_2O_3$ coatings at deposition temperatures higher than 300 °C, being the critical bonding temperature, on a carbon steel substrate to form FeO scale and on an Ni substrate to form NiO scale with a thickness less than 2 μm, with which an adhesive strength higher than 100 MPa can be achieved even on polished flat substrates. Here, the thickness of the oxide scale needs to be optimized to acquire an interface temperature between the scale and the splats to fulfill the chemical bonding requirement and to reduce the grown stress across the interface. Therefore, the excellent adhesive bonding at the interface between the splat and the oxide scale pre-oxidized on the metal substrate can also be explained by the bonding formation model. Thus, it becomes possible that, through the controls of both the pre-oxidation and the deposition temperature, all the interfaces in the ceramic coating system consisting of metal/oxide scale/splat/splat can be bonded chemically to achieve an excellent load-bearing ceramic coating system, which turns out in the form of apparent high adhesive strength.

Different application requirements need different microstructures, from porous ones with limited interface bonding to dense ones with intersplat interface complete

bonding. By taking account of the splat thickness effect on the liquid splat–substrate interface temperature, intersplat bonding can also be adjusted by changing the spray particle size. Therefore, based on the critical bonding temperature concept, the intersplat bonding can be controlled along with other factors influencing the liquid splat–substrate interface temperature. However, with the increase of the intersplat bonding, the residual stress level will be increased. This has been utilized to fabricate TBCs with DVCs. Further work is needed to clarify how such stress levels influence the coating microstructure and performance. Moreover, it is observed that, at a deposition temperature a little higher than the critical bonding temperature, the ceramic coating presents a sintered bulk-like morphology with lamellae fully bonded. It should be pointed out that, during successive deposition of individual splats, the later splats deposit on the previous splats of a rough surface over which many small particles or protrusions are distributed. Sufficient chemical bonding at the intersplat interfaces implies that good wetting can be achieved during liquid splat spreading even on a rough surface. It is necessary to understand how and why such wetting takes place when the interface temperature is higher than $T_g$ at a very high speed. Furthermore, it should be noticed that the present paper presents the knowledge on the bonding formation based on the results for oxide ceramic coatings. The conclusions could be applied to other types of ceramic coatings, such as nitrides, carbides, and silicides, since the primary bonds in oxide ceramic materials are similar to other types of ceramic materials. However, the effect of the oxidation resulting in oxide inclusions on the bonding formation should be taken into consideration.

**Acknowledgements** The present projects are financially supported by National Nature Science Foundationsof China (U1837201) and National Science and Technology Major Project (2019-VII-0007-0147) and 111 project 2.0 (BP0618008).

## References

1. P. Fauchais, J.V.R. Heberlain and M.I. Boulos, *Thermal Spray Fundamentals From Powder to Part*, Springer, New York, 2014.
2. J.R. Davis, *Handbook of Thermal Spray Technology*, ASM International, Materials Park, 2004.
3. A. Vardelle, C. Moreau, J. Akedo, H. Ashrafizadeh, C.C. Berndt, J.O. Berghaus, M. Boulos, J. Brogan, A.C. Bourtsalas, A. Dolatabadi, M. Dorfman, T.J. Eden, P. Fauchais, G. Fisher, F. Gaertner, M. Gindrat, R. Henne, M. Hyland, E. Irissou, E.H. Jordan, K.A. Khor, A. Killinger, Y.C. Lau, C.-J. Li, L. Li, J. Longtin, N. Markocsan, P.J. Masset, J. Matejicek, G. Mauer, A. McDonald, J. Mostaghimi, S. Sampath, G. Schiller, K. Shinoda, M.F. Smith, A.A. Syed, N.J. Themelis, F.L. Toma, J.P. Trelles, R. Vassen, P. Vuoristo, The 2016 Thermal Spray Roadmap. *J. Therm. Spray Technol.*, 2016, **25**(8), p 1376-1440.
4. D.A. Gereman and N.L. Hecht, *Arc Plasma Technology in Materials Science*, Springer , Wien, New York, 1972.
5. L. Pawlowski, *The Science and Engineering of Thermal Spray Coatings*, Wiley, New York, 2008.
6. High-performance Ceramic Coatings: North American Markets and Technologies, BCC Research, Wellesley, MA USA, 2010. Web: www.bccresearch.com
7. D. Matejka and B. Benko, *Plasma Spraying of Metallic and Ceramic Materials*, Wiley, Baffins Lane, Chichester, UK, 1989.
8. C.C. Berndt and R. McPherson, The Adhesion of Plasma Sprayed Ceramic Coatings to Metals, *Materials Science Research, Surface and Interfaces in Ceramic and Ceramic-Metal Systems*, Vol 14, J. Pask, A. Evans Ed., Plenum, New York and London, 1980, p 619-628
9. R. McPherson and B.V. Shafer, Interlamellar Contact within Plasma Sprayed Coatings, *Thin Solid Films*, 1982, **97**, p 201-204.
10. R. McPherson, A Model for the Thermal Conductivity of Plasma Sprayed Ceramic Coatings, *Thin Solid Films*, 1984, **112**, p 89-95.
11. C.-J. Li and A. Ohmori, Relationship between the Structure and Properties of Thermally Sprayed Deposits, *J. Therm. Spray Technol.*, 2002, **11**(3), p 365-374.
12. R.C. Tucker, Structure Property Relationships in Deposits Produced by Plasma Spray and Detonation Gun Techniques, *J. Vac. Sci. Technol.*, 1974, **11**(4), p 725-734.
13. V.V. Sobolev, J.M. Guilemany, J. Nutting and J.R. Miquel, Development of Substrate-Coating Adhesion in Thermal Spraying, *Int. Mater. Rev.*, 1997, **42**(3), p 117-136.
14. R.T. Allsop, T.J. Pitt and J.V. Hardy, The Adhesion of Sprayed Molybdenum, *Metall.*, 1961, **63**, p 125-131.
15. F.N. Longo, Metallurgy of Flame Sprayed Nickel Aluminide Coatings, *Weld. J.* 1966, p 66s-69s.
16. S. Kitahara, A Study of the Bonding Mechanism of Sprayed Coatings, *J. Vac. Sci. Technol.*, 1974, **11**(4), p 747-753.
17. J.M. Houben and G.G.V. Liempd, Metallurgical Interactions of Mo and Steel During Plasma Spraying, Proceedings of 10th International Thermal Spray Conference, May 4-7, 1983 (Essen, Germany), German Welding Institute, 1983, pp. 66-71
18. C.-J. Li, C.-X. Li, G.-J. Yang and Y.-Y. Wang, Examination of Substrate Surface Melting-Induced Splashing during Splat Formation in Plasma Spraying, *J. Thermal Spray Technol.*, 2006, **15**(4), p 717-724.
19. S. Dallaire, Influence of Temperature on the Bonding Mechanism of Plasma-Sprayed Coatings, *Thin Solid Films*, 1982, **95**(3), p 237-244.
20. L. Li, X.X. Wang, G. Wei, A. Vaidya, H. Zhang and S. Sampath, Substrate Melting During Thermal Spray Splat Quenching, *Thin Solid Films*, 2004, **468**, p 113-119. https://doi.org/10.1016/j.tsf.2004.05.073
21. P. Fauchais, M. Fukumoto, A. Vardelle and M. Vardelle, Knowledge Concerning Splat Formation: An Invited Review, *J. Therm. Spray Technol.*, 2004, **13**(3), p 337-360.
22. C. Moreau, P. Cielo and M. Lamontagne, Flattening and Solidification of Thermally Sprayed Particles, *J. Therm. Spray Technol.*, 1992, **1**, p 317-324.
23. A. McDonald, M. Lamontagne, S. Chandra and C. Moreau, Photographing Impact of Plasma-Sprayed Particles on Metal Substrates, *J. Thermal Spray Technol.*, 2006, **15**, p 708-716.
24. S. Goutier, M. Vardelle, P. Fauchais, Last Developments in Diagnostics to Follow Splats Formation during Plasma Spraying, *J. Phys.: Conf. Series*, 2011, **275**, p 012003.
25. V. Pershin, M. Lufitha, S. Chandra and J. Mostaghimi, Effect of Substrate Temperature on Adhesion Strength of Plasma-Sprayed Nickel Coatings, *J. Therm. Spray Technol.*, 2003, **12**, p 370-376.

26. B.N. Kocthkob and U.A. Shestelin, *Plasma Spraying, Moskow Metallurgical Publishing*, Japan-Soviet Communication Publishing Co., Ltd, 1978. (**In Japanese**)
27. E. Kadyrov and V. Kadyrov, Gas Dynamical Parameters of Detonation Powder Spraying, *J. Thermal Spray Technol.*, 1995, **4**(3), p 286-286.
28. V. Shibe and V. Chawla, Erosion Studies of D-gun-sprayed WC-12Co, $Cr_3C_2$-25%NiCr and $Al_2O_3$-13%$TiO_2$ Coatings on ASTM A36 Steel, *J. Thermal Spray Technol.*, 2019, **28**, p 2015-2028.
29. E. Turunen, T. Varis, S.-P. Hannula, A. Vaidya, A. Kulkarni, J. Gutleber, S. Sampath and H. Herman, On the Role of Particle State and Deposition Procedure on Mechanical, Tribological and Dielectric Response of High Velocity Oxy-Fuel Sprayed Alumina Coatings, *Mater. Sci. Eng. A*, 2006, **A415**, p 1-11.
30. G. Johner, V. Wilms, K.K. Schweitzer and P. Adam, Experimental and Theroretical Aspects of Thick Thermal Barrier Coatings for Turbine Applications, Proc. 1st National Thermal Spray Conferene, 14-17 Sept., 1998, Orlando, Florida, ASM International, 1988, pp. 155-166
31. D.M. Gray, Y.C. Lau, C.A. Johnson, M.P. Borom, W.A. Nelson, Thermal Barrier Coatings Having an Improved Columnar Microstructure, United States Patent, 5,830,586, Nov. 3, 1988
32. G.N. Heintze and S. Uematsu, Preparation and Structures of Plasma-Sprayed $\gamma$-and $\alpha$-$Al_2O_3$ Coatings, *Surface Coat. Technol.*, 1992, **50**(3), p 213-222.
33. I.H. Jung, K.K. Bae, M.S. Yang and S.K. Ihm, A Study of the Microstructure of Yttria-Stabilized Zirconia Deposited by Inductively Coupled Plasma Spraying, *J. Thermal Spray Technol.*, 2000, **9**(4), p 463-477.
34. I.-H. Jung, J.-S. Moon, K.-C. Song and M.-S. Yang, Microstructure of Yttria Stabilized Zirconia Deposited by Plasma Spraying, *Surf. Coat. Technol.*, 2004, **180-181**, p 454-457.
35. H.B. Guo, R. Vassen and D. Stover, Atmospheric Plasma Sprayed Thick Thermal Barrier Coatings with High Segmentation Crack Density, *Surf. Coat. Technol.*, 2004, **186**, p 353-363.
36. H.B. Guo, S. Kuroda and H. Murakami, Microstructures and Properties of Plasma-Spayed Segmented Thermal Barrier Coatings, *J. Am. Ceram. Soc.*, 2006, **89**(4), p 1432-1439.
37. H.B. Guo, S. Kuroda and H. Murakami, Segmented Thermal Barrier Coatings Produced by Atmospheric Plasma Spraying Hollow Powders, *Thin Solid Films*, 2006, **506-507**, p 136-139.
38. A. Tricoire, M. Vardelle, P. Fauchais, F. Braillard, A. Malie and P. Bengtsson, Macrocrack Formation in Plasma-Sprayed YSZ TBCs When Spraying Thick Passes, *High Temp. Mater. Process*, 2005, **9**, p 401-413.
39. A. Tricoire, M. Vardelle, P. Fauchais, F. Braillard, A. Malie, P. Bengtsson, New Concepts for Plasma Sprayed Zirconia TBC for Aeronautic Applications, in: E. Lugscheider (Ed.), Thermal Spray Connects: Explore its Surfacing Potential, Proceedings of the 2005 International Thermal Spray Conference, Basil, Switzerland, 2005, pp. 924-928
40. Y.-Z. Xing, C.-J. Li, C.-X. Li and G.-J. Yang, Influence of Through-Lamella Grain Growth on Ionic Conductivity of Plasma-Sprayed Yttria Stabilized Zirconia as an Electrolyte in Solid Oxide Fuel Cells, *J. Power Sour.*, 2008, **176**(1), p 31-38.
41. Y.-Z. Xing, C.-X. Li, C.-J. Li, H.-G. Long and Y.-X. Xie, Microstructure Development of Plasma Sprayed Yttria-Stabilized Zirconia and its Effect on Electrical Conductivity, *Solid State Ionics*, 2007, **179**(27), p 1483-1485.
42. S. Hao, C.-J. Li and G.-J. Yang, Influence of Deposition Temperature on the Microstructures and Properties of Plasma-sprayed $Al_2O_3$ Coatings, *J. Thermal Spray Technol.*, 2011, **20**, p 160-169.
43. G.-J. Yang, C.-X. Li, S. Hao, Y.-Z. Xing, E.-J. Yang and C.-J. Li, Critical Bonding Temperature for the Splat Bonding Formation during Plasma Spraying of Ceramic Materials, *Surf. Coat. Technol.*, 2013, **235**, p 841-847.
44. S.-W. Yao, C.-J. Li, J.-J. Tian, G.-J. Yang and C.-X. Li, Conditions and Mechanisms for the Bonding of a Molten Ceramic Droplet to a Substrate after High-speed Impact, *ACTA Mater.*, 2016, **119**, p 9-25.
45. C.-J. Li, G.-J. Yang and C.-X. Li, Development of the Particle Interface Bonding in Thermal Spray Coatings: A Review, *J. Thermal Spray Technol.*, 2013, **22**(2), p 192-206.
46. A. Hasui, S. Kitahara and T. Fukushima, On Relation between Properties of Coating and Spraying Angle in Plasma Jet Spraying, *Trans. Natl. Res. Inst. Met.*, 1970, **12**, p 9-20.
47. R.C. Dykhuizen, Review of Impact and Solidification of Molten Thermal Spray Droplets, *J. Therm. Spray Technol.*, 1994, **3**, p 351-361.
48. M. Vardelle, A. Vardelle, A.C. Leger, P. Fauchais and D. Gobin, Influence of Particle Parameters at Impact on Splat Formation and Solidification in Plasma Spraying Processes, *J. Thermal Spray Technol.*, 1995, **4**(1), p 50-58.
49. M. Fukumoto, S. Katoh, and I. Okane, Splat Behavior of Plasma Sprayed Particles on Flat Substrate Surface, in: A. Ohmori (Ed.), Thermal Spraying: Current Status and Future Trends, vol. 1, High Temperature Society of Japan, 1995, pp. 353-358
50. M. Fukumoto, I. Ohgitani and T. Yasui, Effect of Substrate Surface Change on Flattening Behaviour of Thermal Sprayed Particles, *Mater. Trans.*, 2004, **45**(6), p 1869-1873.
51. X. Jiang, Y. Wan, H. Herman and S. Sampath, Role of Condensates and Adsorbates on Substrate Surface on Fragmentation of Impinging Molten Droplets during Thermal Spray, *Thin Solid Films*, 2001, **385**, p 132-141.
52. C.-J. Li and J.-L. Li, Evaporated-Gas-Induced Splashing Model for Splat Formation during Plasma Spraying, *Surf. Coat. Technol.*, 2004, **184**(1), p 13-23.
53. P. Fauchais, M. Vardelle, A. Vardelle and L. Bianchi, Plasma Spray: Study of the Coating Generation, *Ceram. Int.*, 1996, **22**, p 295-303.
54. A. McDonald, C. Moreau and S. Chandra, Thermal Contact Resistance between Plasma-Sprayed Particles and Flat Surfaces, *Int. J. Heat Mass Transf.*, 2007, **50**, p 1737-1749.
55. C.-J. Li, A.Ohmori and Y.Harada, 1995, Experimental Investigation of the Morphologies of Plasma Sprayed Copper Splats, Proceedings of 14th International Thermal Spray Conference (14th ITSC), 1995, Japan High Temperature Society, ed. A.Ohmori, pp. 333-339
56. C. Moreau, P. Gougeon and M. Lamontagne, Influence of Substrate Preparation on the Flattening and Cooling of Plasma-Sprayed Particles, *J. Thermal Spray Technol.*, 1995, **4**, p 25-33.
57. C.-J. Li, H.-L. Liao, P. Gougeon, G. Montavon and C. Coddet, Effect of Reynolds Numbers of Molten Particle on Splat Formation in Plasma Spraying, *Thermal Spray: Advancing the Science and Applying the Technology*, (Ed.) C. Moreau and B. Marple, Published by ASM international, Materials Park, OH-USA, 2003, pp. 875-882
58. C.-J. Li, Effect of the Surface Adsorbates on the Morphology of Plasma-Sprayed Splats, Tagungsband Conference Proceedings (2005 Int. Thermal Spray Conf.], Ed. E. Lugscheider, May 2-5, Bussel, Switzerland, German Welding Research Institute, 2005, Germany, pp. 311-319
59. S. Goutier, M. Vardelle and P. Fauchais, Comparison between Metallic and Ceramic Splats: Influence of Viscosity and Kinetic Energy on the Particle Flattening, *Surf. Coat. Technol.*, 2013, **235**, p 657-668.
60. L. Bianchi, A. Grimaud, F. Blein, P. Lucchese and P. Fauchais, Comparison of Plasma-Sprayed Alumina Coatings by RF and DC Plasma Spraying, *J. Thermal Spray Technol.*, 1995, **4**, p 59-66.

61. S. Bhusal, C. Zhang, J. Bustillos, P. Nautiyal, B. Boesl and A. Agarwa, A computational approach for predicting microstructure and mechanical properties of plasma sprayed ceramic coatings from powder to bulk, *Surf. Coat. Technol.*, 2019, **374**, p 1-11.
62. Y.G. Zhang, M. Hyland, A.T. Tran and S. Matthews, Effect of Substrates Temperatures on the Spreading Behavior of Plasma Sprayed Ni and Ni-20 wt.% Cr Splats, *J. Thermal Spray Technol.*, 2016, **25**(1-2), p 71-81.
63. J. Madejski, Solidification of Droplets on a Cold Substrate, *Int. J. Heat Mass Transf.*, 1976, **19**, p 1009-1013.
64. H. Jones, Cooling, Freezing and Substrate Impact of Droplets Formed by Rotary Atomization, *J. Phys. D*, 1971, **4**, p 1657-1660.
65. G. Trapaga, E.F. Matthys, J.J. Vaencia and J. Szekely, Fluid Flow, Heat Transfer, and Solidification of Molten Metal Droplets Impacting on Substrate: Comparison of Numerical and Experimental Results, *Metall. Trans. B*, 1992, **23B**, p 701-718.
66. M. Bertagnolli, M. Marchese and G. Jacucci, Modeling of Particles Impacting on a Rigid Substrate under Plasma Spraying Conditions, *J. Thermal Spray Technol.*, 1995, **4**, p 41-49.
67. H. Liu, E.J. Lavernia and R.H. Rangel, Numerical Simulation of Impingement of Molten Ti, Ni, and W Droplets on a Flat Substrate, *J. Thermal Spray Technol.*, 1993, **2**, p 369-378.
68. C.-J. Li and J.-L. Li, Transient Contact Pressure during Flattening of Thermal Spray Droplet and its Effect on Splat Formation, *J. Therm. Spray Technol.*, 2004, **13**(2), p 229-238.
69. C.-J. Li, H.L. Liao, P. Gougeon, G. Montavon and C. Coddet, Experimental Determination of the Relationship between Flattening Degree and Reynolds Number for Spray Molten Droplets, *Surf. Coat. Technol.*, 2005, **191**(2-3), p 375-383.
70. L. Bianchi, A.C. Leger, M. Vardelle, A. Vardelle and P. Fauchais, Splat Formation and Cooling of Plasma-Sprayed Zirconia, *Surf. Coat. Technol.*, 1997, **305**, p 35-47.
71. H. Jones, Splat Cooling and Metastable Phases, *Rep. Progr. Phys.*, 1973, **36**(11), p 1425.
72. R. McPherson, Formation of Metastable Phase in Flame- and Plasma-Prepared Alumina, *J. Mater. Sci.*, 1973, **8**, p 851-858.
73. S. Safai and H. Herman, Plasma-Sprayed Materials, In Ultrarapid Quenching of Liquid Alloys, Treatise on Materials Science and Technology, Vol.20, Ed. H. Herman, 1981, pp.183-214.
74. C. Moreau, P. Cielo, M. Lamontagne, S. Dallaire and M. Vardelle, Impacting Particle Temperature Monitoring during Plasma Spray Deposition, *Meas. Sci. Technol.*, 1990, **1**, p 807-814.
75. C. Moreau, M. Lamontagne and P. Cielo, Influence of the Coating Thickness on the Cooling Rate of Plasma-Sprayed Particles Impinging on a Substrate, in Proceedings of the Fourth National Thermal Spray Conference, Pittsburgh, PA, USA, 4-12 May 1991, ASM International, 1992, pp 237-243
76. S. Goutier, M. Vardelle, J.C. Labbe and P. Fauchais, Flattening and Cooling of Millimeter and Micrometer-Sized Alumina Drops, *J. Thermal Spray Technol.*, 2011, **20**, p 59-67.
77. S. Valette, R. Bernardie, J. Absi and P. Lefort, Elaboration and Characterisation of Plasma Sprayed Alumina Coatings on Nickel with Nickel Oxide Interlayer, *Surf. Coat. Technol.*, 2021, **416**, p 127-159.
78. J.-J. Tian, S.-W. Yao, X.-T. Luo, C.-X. Li and C.-J. Li, An Effective Approach for Creating Metallurgical Self-Bonding in Plasma-Spraying of NiCr-Mo Coating by Designing Shell-Core-Structured Powders, *ACTA Mater.*, 2016, **110**, p 19-30.
79. X.-Y. Dong, X.-T. Luo, S.-L. Zhang and C.-J. Li, A Novel Strategy for Depositing Dense Self-fluxing Alloy Coatings with Sufficiently Bonded Splats by One-Step Atmospheric Plasma Spraying, *J. Thermal Spray Technol.*, 2020, **29**(1), p 173-184.
80. Y. Lahmar-Mebdoua, A. Vardelle, P. Fauchais and D. Gobin, Modelling the Nucleation Process in Alumina Lamellae Deposited on a Steel Substrate, *Int. J. Therm. Sci.*, 2010, **49**, p 522-552.
81. F. Ferguen, P. Fauchais, A. Vardelle and D. Gobin, Numerical Investigation of Impact and Solidification YSZ Droplets Plasma-Sprayed onto a Substrate: Effect of Thermal Properties and Roughness, Advanced Ceramics Coatings and Interfaces III, eds. H.T Lin and D.M Zhu, American Ceramic Society, 2009, pp.159-170
82. O.G. Angel, Waterdrop Collisions with Solid Surfaces, *J. Res. Natl. Bure. Stand.*, 1955, **54**, p 281-298.
83. V.V. Sobolev and J.M. Guilemany, Droplet-Substrate Impact Interaction in Thermal Spraying, *Mater. Lett.*, 1996, **28**, p 33l-335.
84. J.-L. Li, Splatting Behavior of the Droplet Impinging on Substrate in Plasma Spraying, Ph.D Thesis, Xi'an Jiaotong University, 1999
85. W. Tillmann, O. Khalil and I. Baumann, Influence of spray gun parameters on inflight particle's characteristics, the splat-type distribution, and microstructure of plasma-sprayed YSZ coatings, *Surf. Coat. Technol.*, 2021, **406**, p 126705.
86. J.F. Bisson, C. Moreau, M. Dorfman, C. Dambra and J. Mallon, Influence of Hydrogen on the Microstructure of Plasma-Sprayed Yttria-Stabilized Zirconia Coatings, *J. Thermal Spray Technol.*, 2005, **14**, p 85-90.
87. V. Srinivasan and S. Sampath, Estimation of Molten Content of the Spray Stream from Analysis of Experimental Particle Diagnostics, *J. Thermal Spray Technol.*, 2005, **19**, p 476-483.
88. Y.-Z. Xing, Y. Li, C.-J. Li, C.-X. Li and G.-J. Yang, Influence of Substrate Temperature on Microcracks Formation in Plasma-Sprayed Yttria-Stabilized Zirconia Splats, *Key Eng. Mater.*, 2008, **373-374**, p 69-72.
89. A.T.T. Tran, M.M. Hyland, K. Shinoda and S. Sampath, Inhibition of Molten Droplet Deposition by Substrate Surface Hydroxides, *Surf. Coat. Technol.*, 2011, **206**, p 1283-1292.
90. A.T.T. Tran, M.M. Hyland, K. Shinoda and S. Sampath, Influence of Substrate Surface Conditions on the Deposition and Spreading of Molten Droplets, *Thin Solid Films*, 2011, **519**, p 2445-2456.
91. S. Brossard, P.R. Munroe, A.T.T. Tran and M.M. Hyland, Study of the Effects of Surface Chemistry on Splat Formation for Plasma Sprayed NiCr onto Stainless Steel Substrates, *Surf. Coat. Technol.*, 2010, **204**, p 1599-1607.
92. A.T.T. Tran, M.M. Hyland, T. Qiu, B. Withy and B.J. James, Effects of Surface Chemistry on Splat Formation During Plasma Spraying, *J. Thermal Spray Technol.*, 2008, **17**(5-6), p 2008-637.
93. J. Wang, C.-J. Li, G.-J. Yang and C.-X. Li, Effect of Oxidation on the Bonding Formation of Plasma-sprayed Stainless Steel Splats onto Stainless Steel Substrate, *J. Thermal Spray Technol.*, 2017, **26**(1-2), p 47-59.
94. Y. Tanaka and M. Nakashima, M. Fukumoto, Effect of Substrate Surface Condition on Flattening Behavior of Thermal Sprayed Ceramic Particles. *Quarterly J. Japan Weld. Soc.*, 2002, **20**, 317–321. (**In Japanese**)
95. Y. Zhang, M. Hyland, A.T. Tran and S. Matthews, Effect of Substrates Temperatures on the Spreading Behavior of Plasma Sprayed Ni and Ni-20 wt.% Cr Splats, *J. Thermal Spray Technol.*, 2016, **25**(1-2), p 71-81.
96. A.A. Syed, P. Denoirjean, A. Denoirjean, J.C. Labbe and P. Fauchais, Influence of Substrate Surface Preheating Stage on the Morphology and Flattening of Splats, *High Temp. Mater. Process.*, 2003, **7**, p 195-203.
97. A.A. Syed, A. Denoirjean, B. Hannoyer, P. Fauchais, P. Denoirjean, A.A. Khan and J.C. Labbe, Influence of Substrate

Surface Conditions on the Plasma Sprayed Ceramic and Metallic Particles Flattening, *Surf. Coat. Technol.*, 2005, **200**, p 2317-3233.
98. S. Kuroda and T.W. Clyne, The Quenching Stress in Thermally Sprayed Coatings, *Thin Solid Films*, 1991, **200**, p 49-66.
99. L. Chen, G.-J. Yang and C.-J. Li, Hierarchical Formation of Intrasplat Cracks in Thermal Spray Ceramic Coatings, *J. Thermal Spray Technol.*, 2016, **25**, p 959-970.
100. Jyun Miyase, *Japan Thermal Spray Associate, Handbook of Thermal Spray*, Auto Press, Tokyo, 1985. (**In Japanese**)
101. D.T. Gawne, B.J. Griffiths and G. Dong, The influence of Pretreatment on the Adhesion of Ceramic Coatings on Steel, *Trans. IMF*, 1997, **75**(6), p 205-207.
102. N. Iwamoto, Y. Makino, N. Umesaki, S. Endo, H. Kobayashi, The Effect of Pretreatments of Metals on Bond Adhesion, in Proceedings of the 10th International Thermal Spray Conference, 80, DVS, Dusseldorf, Germany, 1983, pp. 18-22.
103. B. Wielage, J. Drozak, Bonding Problems by APS-sprayed Coatings, TS90 Thermal Spray Conference, August 29-31, 1990, Essen, DVS, Dusseldorf, Germany, 1990, pp 243-246.
104. T.J. Roseberry, F.W. Boulger, A Plasma Flame Spray Handbook, Report No.MT-043, US, Department of Commerce, National Technical Information Service, Springfield, US, 1977
105. W. Funk, F, Goebe, M. Mauz, The Influence of Substrate Temperature on the Bond Strength of Plasma Sprayed Oxide Ceramics, in 1st Plasma Technic Symposium, Vol.1, H. Eschnauer, P. Huber, A.R. Nicoll, S. Sandmeier (Eds), Plasma-Technic AG, Wohlen, Switzerland, pp 59-66.
106. R.B. Heimann, O. Grabmann, T. Zumbrink and H.P. Jennissen, Biometric Processes during in Vitro Leaching of Plasma-Sprayed Hydroxyapatite Coatings for Endo-Prosthetic Applications, *Mater. Siss. U. Werkstofftech*, 2001, **32**, p 913-921.
107. R.S. Lima, B.R. Marple, K.A. Khor, H. Li, P. Cheang, Mechanical Properties, Microstructural Characteristics and In-Vitro Behavior of APS Sprayed Nanostructured and Conventional Hydroxyapatite Coatings, in the Proceedings of 2004 International Thermal Spray Conference, ISBN-3-87155-792-7, DVS , 2004, Dusseldorf, Germany
108. Y. Yang, Z. Liu and Y. Chuang, Measurements of Residual Stress and Bond Strength of Plasma Sprayed Laminated Coatings, *Surf. Coat. Technol.*, 1997, **89**, p 97-100.
109. N.R. Shankar and C.C. Berndt, H, Herman, Failure and Acoustic Emission Response of Plasma Sprayed $ZrO_2$-8 wt% $Y_2O_3$ Coatings, *Ceramic Eng. Sci. Process.*, 1982, **3**, p 772-792.
110. J. Pech and B. Hannoyer, Influence of Oxide Layer Promoted by d.c. Plasma Preheating on the Adhesion Coating and Role of the Initial Surface Pretreatment. Surf. Interface Anal. **30**, 585-588 (2000)
111. L. Gyenis, A. Grimaud, O. Betoule, F. Monerie-Moulin, and P. Fauchais, Influence of Temperature Control during Spraying on Hardness and Cohesion of Alumina Coating, in Proceedings of 2nd Plasma-Technic-Symposium, Vol.1, Lucerne, Switzerland, June 5-7, 1991, eds. S. Blum-Sandmeier, H. Eschnauer, P. Huber, A.R. Nicill, pp. 95–101
112. A. Maitre, A. Denoirjean, P. Fauchais and P. Lefort, Plasma-Jet Coating of Preoxidized XC38 Steel: Influence of the Nature of the Oxide Layer, *Phys. Chem. Chem. Phys.*, 2002, **4**, p 3887-3893.
113. L. Bianchi,A. Denoirjean, P. Fauchais, O. Postel, Generation of Alumina Plasma Sprayed Coatings on Alumina Substances, In Thermal Spray: Practical Solutions for Engineering Problems, Proceedings of 9th National Thermal Spray Conference & Exposition, C.C. Berndt (ed), ASM International, Materials Park, Ohio-USA, 1996, pp. 749-755
114. A.S. Khanna, Introduction to High Temperature Oxidation and Corrosion, ASM International, Materials Park, 2002, pp. 83-86
115. S. Valette, G. Trolliard, A. Denoirjean and P. Lefort, Iron/Wustite/Magnetite/Alumina Relatisonships in Plasma Coated Steel: A TEM Study, *Solid State Ionics*, 2007, **178**, p 429-437.
116. S. Valette, A. Denoirjean and P. Lefort, Plasma Sprayed Steel: Adhesion of an Alumina Film via a Wustite Interlayer, *Surf. Coat. Technol.*, 2008, **202**, p 2603-2611.
117. C.U. Hardwicke and Y.-C. Lau, Advances in Thermal Spray Coatings for Gas Turbines and Energy Generation: A Review, *J. Thermal Spray Technol.*, 2013, **22**, p 564-576.
118. L. Sun, Thermal Spray Coatings on Orthopedic Devices: When and How the FDA Reviews Your Coatings, *J. Therm Spray Technol.*, 2018, **27**, p 1280-1290.
119. C.-J. Li, J. Zou, H.-B. Huo, J.-T. Yao and G.-J. Yang, Microstructure and Properties of Porous Abradable Alumina Coatings Flame-Sprayed with Semi-molten Particles, *J. Thermal Spray Technol.*, 2016, **25**, p 264-272.
120. C.-J. Li and W.-Z. Wang, Quantitative Characterization of Lamellar Microstructure of Plasma-Sprayed Ceramic Coatings through Visualization of Voids Distribution, *Mater. Sci. Eng A*, 2004, **386**(1-2), p 10-19.
121. V. Wilm, H.Herman, Crystallography and Microstructure of Equilibrium and Metastable Phases Resulting from Plasma Spraying of Ceramic Coatings, in Proceedings of 8th International Thermal Spray Conf,, Miami Beach, Florida, American Welding Society, 1976, pp. 236-243
122. H.D. Steffens and U. Fischer, Correlation Between Microstructure and Physical Properties of Plasma Sprayed Zirconia Coatings, in Proceedings of 2nd National Thermal Spray Conference, ASM International, Materials Park, OH, 1989, pp. 167-73
123. I. Sevostianov and M. Kachanov, Modeling of the Anisotropic Elastic Properties of Plasma-Sprayed Coatings in Relation to Their Microstructure, *Acta Mater.*, 2000, **48**, p 1361-1370.
124. A.J. Allen, J. Ikavsky, G.G. Long, J.S. Wallace, C.C. Berndt and H. Herman, Microstructural Characterization of Yttria-stabilized Zirconia Plasma-Sprayed Deposits Using Multiple Small-Angle Neutron Scattering, *Acta Mater.*, 2001, **49**, p 1661-1675.
125. Y. Arata, A. Ohmori and C.-J. Li, Characteristics of Metal Electroplating to Plasma Sprayed Ceramic Coatings, *Trans. Jpn. Weld. Res. Inst.*, 1987, **16**, p 259-265.
126. Y. Arata, A .Ohmori and C.-J. Li, Study on the Structure of Plasma Sprayed Ceramic Coating by Using Copper Electroplating, in Proceedings of International Symposium on Advanced Thermal Spraying Technology and Allied Coatings (ATTAC'88), Osaka, 13-15 May 1988, Japan High Temperature Society, 1988, pp. 205-210
127. A. Ohmori, C.-J. Li and Y. Arata, Influence of Plasma Spray Conditions on the Structure of $Al_2O_3$ Coatings, *Trans. Jpn. Weld. Res. Inst.*, 1990, **19**, p 259-270.
128. A. Ohmori, C.-J. Li, and Y. Arata, Structure of Plasma-Sprayed Alumina Coatings Revealed by Using Copper Electroplating, in Thermal Spray Coating, Properties, Processes and Applications, T.F. Bernecki, ed., ASM International, Materials Park, OH, 1992, pp. 105-13
129. A. Ohmori and C.-J. Li, Quantitative Characterization of the Structure of Plasma Sprayed $Al_2O_3$ Coating by Using Copper Electroplating, *Thin Solid Films*, 1991, **201**, p 241-252.
130. W.Z. Wang, Quantitative Characterization of Lamellar Microstructure of Plasma Sprayed Coatings and Relationship between Lamellar Microstructure and Properties of Coatings, Xi'an Jiaotong University, Ph.D., Thesis, 2004
131. C.-J. Li, W.-Z. Wang and Y. He, Dependency of Fracture Toughness of Plasma-Spray $Al_2O_3$ Coatings on Lamellar Structure, *J. Thermal Spray Technol.*, 2004, **13**(3), p 425-431.

132. C.-J. Li, A. Ohmori and R. McPherson, The Relationship between Microstructure and Young's Modulus of Thermally Sprayed Ceramic Coatings, *J. Mater. Sci.*, 1997, **32**, p 997-1004.
133. A. Ohmori and C.-J. Li, The structure of thermally sprayed ceramic coatings and its dominant effect on the coating properties, *Plasma Spraying, Theory and Applications*. S. Surayanarayanan Ed., World Scientific, Singapore, 1993, p 179-200
134. Y.Z. Xing, C.-J. Li, Q. Zhang, C.-X. Li and G.-J. Yang, Influence of Microstructure on the Ionic Conductivity of Plasma-Sprayed Yttria-Stabilized Zirconia Deposits, *J. Am. Ceram. Soc.*, 2008, **91**(12), p 3931-3936.
135. C.-J. Li, G.-J. Yang and A. Ohmori, Relationship between Particle Erosion and Lamellar Microstructure for Plasma Sprayed Alumina Coatings, *Wear*, 2006, **260**, p 1166-2117.
136. A. Cipitria, I.O. Golosnoy and T.W. Clyne, A Sintering Model for Plasma-Sprayed Zirconia TBCs. Part I: Free-Standing Coatings, *ACTA Mater.*, 2009, **57**(4), p 980-992.
137. S. Paul, A. Cipitria, S.A. Tsipas and T.W. Clyne, Sintering Characteristics of Plasma Sprayed Zirconia Coatings Containing Different Stabilisers, *Surf. Coat. Technol.*, 2009, **203**(8), p 1069-1074.
138. W.G. Chi, S. Sampath and H. Wang, Microstructure-Thermal Conductivity Relationships for Plasma-Sprayed Yttria-Stabilized Zirconia Coatings, *J. Am. Ceram. Soc.*, 2008, **91**(8), p 2636-2645.
139. Y.Z. Wang, W. Wu, X.B. Zheng, Y. Zeng, M.J. Ding and C.G. Zhang, Relationship Between the Microstructure and Thermal Conductivity of Plasma-Sprayed $ZrO_2$ Coatings, *J. Therm Spray Technol.*, 2011, **20**(6), p 1177-1182.
140. Y. Tan, J.P. Longtin, S. Sampath and H. Wang, Effect of the Starting Microstructure on the Thermal Properties of As-Sprayed and Thermally Exposed Plasma-Sprayed YSZ Coatings, *J. Am. Ceram. Soc.*, 2009, **92**(3), p 710-716.
141. R. Dutton, R. Wheeler, K.S. Ravichandran and K. An, Effect of Heat Treatment on the Thermal Conductivity of Plasma-Sprayed Thermal Barrier Coatings, *J. Therm. Spray Technol.*, 2000, **9**(2), p 204-209.
142. N. Markocsan, P. Nylen, J. Wigren, X.H. Li and A. Tricoire, Effect of Thermal Aging on Microstructure and Functional Properties of Zirconia-Base Thermal Barrier Coatings, *J. Therm. Spray Technol.*, 2009, **18**(2), p 201-208.
143. H.J. Ratzer-Scheibe and U. Schulz, The Effects of Heat Treatment and Gas Atmosphere on the Thermal Conductivity of APS and EB-PVD PYSZ Thermal Barrier Coatings, *Surf. Coat. Technol.*, 2007, **201**(18), p 7880-7888.
144. D.M. Zhu and R.A. Miller, Thermal Conductivity and Elastic Modulus Evolution of Thermal Barrier Coatings under High Heat Flux Conditions, *J. Therm. Spray Technol.*, 2000, **9**(2), p 175-180.
145. A.D. Jadhav, N.P. Padture, E.H. Jordan, M. Gell, P. Miranzo and E.R. Fuller, Low-Thermal-Conductivity Plasma-Sprayed Thermal Barrier Coatings with Engineered Microstructures, *Acta Mater.*, 2006, **54**(12), p 3343-3349.
146. S. Paul, A. Cipitria, I.O. Golosnoy, L. Xie, M.R. Dorfman and T.W. Clyne, Effects of Impurity Content on the Sintering Characteristics of Plasma-Sprayed Zirconia, *J. Therm. Spray Technol.*, 2007, **16**(5-6), p 798-803.
147. R.W. Trice, Y.J. Su, J.R. Mawdsley, K.T. Faber, A.R. De Arellano-Lopez, H. Wang and W.D. Porter, Effect of Heat Treatment on Phase Stability, Microstructure, and Thermal Conductivity of Plasma-Sprayed YSZ, *J. Mater. Sci.*, 2002, **37**(11), p 2359-2365.
148. W.W. Zhang, G.R. Li, Q. Zhang, G.J. Yang, G.W. Zhang and H.M. Mu, Self-Enhancing Thermal Insulation Performance of Bimodal-Structured Thermal Barrier Coating, *J. Therm. Spray Technol.*, 2018, **27**(7), p 1064-1075.
149. J. Wu, X.Z. Wei, N.P. Padture, P.G. Klemens, M. Gell, E. Garcia, P. Miranzo and M.I. Osendi, Low-Thermal-Conductivity Rare-Earth Zirconates for Potential Thermal-Barrier-Coating Applications, *J. Am. Ceram. Soc.*, 2002, **85**(12), p 3031-3035.
150. P. Fauchais, M. Vardelle, A. Vardelle, and J.F. Coudert, Plasma Spraying of Ceramic Particles in Argon-Hydrogen D.C. Plasma Jets: Modeling and Measurements of Particles in Flight Correlation with Thermophysical Properties of Sprayed Layers, *Metall. Trans. B*, 1989, **20B**, p 263-276.
151. H.D. Steffens, M. Mack and R. Lauterbach, Measurement of Particle Velocities for an Analytical Model of Low Pressure Plasma Jets, in Proceedings of 1st Plasma Technik Symposium, Lucerne, Switzerland, May 18th to 20th, 1988, pp. 67-76
152. M.F. Smith, Laser Measurement of Particle Velocities in Vacuum Plasma Spray Deposition, in Proceedings of 1st Plasma Technik Symposium, Lucerne, Switzerland, May 18th to 20th, 1988, pp. 77-85
153. E. Kadyrov, Gas-Particle Interaction in Detonation Spraying Systems, *J. Thermal Spray Technol.*, 1996, **5**(2), p 185-95.
154. A. Kulkarni, J. Gutleber, S. Sampath, A. Goland, W.B. Lindquist, H. Herman, A.J. Allen and B. Dowd, Studies of the Microstructure and Properties of Dense Ceramic Coatings Produced by High-Velocity Oxygen-Fuel Combustion Spraying, *Mater. Sci. Eng. A*, 2004, **369**, p 124-137.
155. M.P. Planche, S. Costil, C. Verdy and C. Coddet, Different Spray Processes for Different $Al_2O_3$ Coating Properties, *Appl. Phys. A. Mater. Sci. Process*, 2010, **99**, p 665-671.
156. A. Vardelle, M. Vardelle, R. McPherson, and P. Fauchais, Study of the Influence of Particle Temperature and Velocity Distribution Within a Plasma Jet Coating Formation, in Proceedings of the 9th International Thermal Spraying Conference, Nederland Inst. Voor Lastetechnik, Hague, The Netherlands, 1980, pp. 155-61
157. M. Vardelle, A. Vardelle, and P. Fauchais, Study of Trajectories and Temperatures of Powders in a D.C. Plasma Jet—Correlation With Alumina Sprayed Coatings, in Proceedings of the 10th International Thermal Spraying Conference, German Welding Society, Essen, Germany, 1983, pp. 88-92
158. J. Wang, X.-T. Luo, C.-J. Li, N. Ma, M. Takahashi, Effect of Substrate Temperature on the Microstructure and Interface Bonding Formation of Plasma Sprayed Ni20Cr Splat, *Surf. Coat. Technol.*, 2019, **371**, p 36-46.
159. P. Saravanan, V. Selvarajan, M.P. Srivastava, D.S. Rao, S.V. Joshi and G. Sundararaja, Study of Plasma- and Detonation Gun-Sprayed Alumina Coatings Using Taguchi Experimental Design, *J. Therm. Spray Technol.*, 2000, **9**, p 505-512.
160. Y. Fukuda, H. Yamasaki, M. Kumonn, M. Kawahara and H. Kimura, Detonation Coating for Coal Fired Boiler Tubes, Proceedings of International Symposium on Advanced Thermal Spraying Technology and Allied Coatings (ATTAC'88), Osaka, 13-15 May 1988, Japan High Temperature Society, 1988, pp. 49-54.
161. C.-J. Li and A. Ohmori, The Lamellar Structure of a Detonation Gun Sprayed $Al_2O_3$ Coating, *Surf. Coat. Technol.*, 1996, **82**, p 254-258.
162. P.S. Babu, D.S. Rao, G.V.N. Rao and G. Sundararajan, Effect of Feedstock Size and its Distribution on the Properties of Detonation Sprayed Coatings, *J. Thermal Spray Technol.*, 2007, **16**(2), p 281-290.
163. C.-J. Li, A. Ohmori and Y. Arata, Effect of Spray Methods on the Lamellar Structure of $Al_2O_3$ Coatings, *Thermal Spray, Current Status and Future Trends*. A. Ohmori Ed., Japan High Temperature Society, Osaka, Japan, 1995, p 501-506.
164. N. Branland, E. Meillot, P. Fauchais, A. Vardelle, F. Gitzhofer and M. Boulos, Relationships between Microstructure and

Electrical Properties of RF and DC Plasma-Sprayed Titania Coatings, *J. Thermal Spray Technol.*, 2006, **15**(1), p 53-62.
165. J. Colmenares-Angulo, K. Shinoda, T. Wentz, W. Zhang, Y. Tan and S. Sampath, On the Response of Different Particle State Sensors to Deliberate Process Variations, *J. Thermal Spray Technol.*, 2011, **20**, p 1035-1048.
166. A. Kulkarni, J. Gutleber, S. Sampath, A. Goland, W.B. Lindquist, H. Herman, A.J. Allen and B. Dowd, Studies of the Microstructure and Properties of Dense Ceramic Coatings Produced by High-Velocity Oxygen-Fuel Combustion Spraying, *Mater. Sci. Eng. A*, 2004, **A369**, p 124-137.
167. A. Kulkarni, S. Sampath, A. Goland and H. Herman, Computed Microtomography Studies to Characterize Microstructure-Property Correlations in Thermal Sprayed Alumina Deposits, *Scripta Mater.*, 2000, **43**, p 471-476.
168. Y.J. Su, H. Wang, W.D. Porter, A.R. de Arellano Lopez, K.T. Faber, Thermal Conductivity and Phase Evolution of Plasma-Sprayed Multilayer Coatings. *J. Mater. Sci.*, 2001, **36**, p 3511–3518.
169. S. Costil. C.Verdy, R. Bolot and C. Coddet, On the Role of Spraying Process on Microstructural, Mechanical, and Thermal Response of Alumina Coatings. *J. Thermal Spray Technol.*, 2007, **16**, p 839-843.
170. G.M. Smith, A. Smith and S. Sampath, Fracture Toughness of Thermal Spray Ceramics: Measurement Techniques and Processing Dependence, *J. Thermal Spray Technol.*, 2018, **27**, p 1076-1089.
171. R.C. Tucker and M.O. Price, The Effect of Angle of Deposition on the Properties of Selected Detonation Gun Coatings, in Proceedings of International Symposium on Advanced Thermal Spraying Technology and Allied Coatings (ATTAC'88), Osaka, 13-15 May 1988, Japan High Temperature Society, 1988, p 61-71
172. H.T. Litter and L.C. Drake, Pore Size Distribution of Porous Materials, Pressure Porosometer and Determination of Macro-Size Distribution, *Inds. Chem. Eng.*, 1954, **17**, p 782-786.
173. R. McPherson, The Relationship between the Mechanism of Formation, Microstructure and Properties of Plasma-Sprayed Coatings, *Thin Solid Films*, 1981, **83**, p 297-310.
174. A. Feuerstein, J. Knapp, T. Taylor, A. Ashary, A. Bolcavage and N. Hitchman, Technical and Economical Aspects of Current Thermal Barrier Coating Systems for Gas Turbine Engines by Thermal Spray and EBPVD: A Review, *J. Thermal Spray Technol.*, 2008, **17**, p 199-213.
175. T. Liu, E.-J. Yang, G.-J. Yang, C.-X. Li and C.-J. Li, The Interface Bonding Formation during Plasma Spraying of $La_2Zr_2O_7$ Coating, *Mater. Res. Innov.*, 2014, **8**(S4), p S973-S978.
176. E.-J. Yang, X.-T. Luo, G.-J. Yang, C.-J. Li and M. Takahashi, Impact of Deposition Temperature on Crystalline Structure of Plasma-Sprayed $Al_2O_3$ Splats Revealed by FIB-HRTEM Technique, *Ceram. Int.*, 2016, **42**(1), p 853-860.
177. E.-J. Yang, X.-T. Luo, G.-J. Yang, C.-J. Li and M. Takahashi, Epitaxial Grain Growth during 8YSZ Splat Formation on Polycrystalline YSZ Substrates by Plasma Spraying, *Surf. Coat. Technol.*, 2015, **274**, p 37-43.
178. C.-J. Li, Q.-L. Zhang, S.-W. Yao, G.-J. Yang and C.-X. Li, Plasma Spraying of Dense Ceramic Coating with Fully BondedLamellae Through Materials Design Based on the Critical Bonding Temperature Concept, *J. Thermal Spray Technol.*, 2019, **28**(1-2), p 53-62.
179. R. Chen, S.-L. Zhang, C.-J. Li and C.-X. Li, Plasma-Sprayed High-Performance $(Bi_2O_3)_{0.75}(Y_2O_3)_{0.25}$ Electrolyte for Intermediate-Temperature Solid Oxide Fuel Cells (IT-SOFCs), *J. Thermal Spray Technol.*, 2021, **30**, p 196-204.
180. H. Liu, W. Chen, R. Pan, Z. Shan, A. Qiao, J.W.E. Drewitt, L. Hennet, S. Jahn, D.P. Langstaff, G.A. Chass, H. Tao, Y. Yue and G.N. Greaves, From Molten Calcium Aluminates through Phase Transitions to Cement Phases, *Adv. Sci.*, 2020, **7**, p 1902209.
181. J. Orava, A.L. Greer, B. Gholipour, D.W. Hewak and C.E. Smith, Characterization of Supercooled Liquid $Ge_2Sb_2Te_5$ and its Crystallization by Ultrafast-Heating Calorimetry, *Nature Mater.*, 2012, **11**, p 279-283.
182. V.P. Elyutin, V.I. Kostikov, B.S. Minton and Y.A. Nagibin, Viscosity of Alumina, *Russ. J. Chem.*, 1969, **43**, p 316.
183. C.A. Angell, Structural Instability and Relaxation in Liquid and Glassy Phases near the Fragile liquid Limit, *J. Non-Cryst. Solids*, 1988, **102**, p 205-221.
184. P.G. Debenedetti and F.H. Stillinger, Supercooled Liquids and the Glass Transition, *Nature*, 2001, **410**, p 259-267.
185. W.H. Wang, The Nature and Properties of Amorphous Matter, *Prog. Phys*, 2013, **33**, p 177-351. (**In Chinese**)
186. D. Holland-Moritz, T. Schenk, V. Simonet, R. Bellissent, P. Convert, T. Hansen and D. Herlach, Short-Range Order in Undercooled Metallic Liquids, *Mater. Sci. Eng. A*, 2004, **A375**, p 98-103.
187. Y. Hu, F. Li, M. Li, H. Bai and W. Wang, Five-Fold Symmetry as Indicator of Dynamic Arrest in Metallic Glass-Forming Liquids, *Nat. Commun.*, 2015, **6**, p 8310.
188. C.P. Royall, S.R. Williams, T. Ohtsuka and H. Tanaka, Direct Observation of a Local Structural Mechanism for Dynamic Arrest, *Nat. Mater.*, 2008, **7**, p 556-561.
189. J. Orava and A.L. Greer, Fast and Slow Crystal Growth Kinetics in Glass-Forming Melts, *J. Chem. Phys.*, 2014, **140**, p 214504.
190. S.-W. Yao, T. Liu, C.-J. Li, G.-J. Yang and C.-X. Li, Epitaxial Growth during the Rapid Solidification of Plasma-Sprayed Molten $TiO_2$ Splat, *ACTA Mater.*, 2017, **134**, p 66-80.
191. L. Li, B. Kharas, H. Zhang and S. Sampath, Suppression of Crystallization during High Velocity Impact Quenching of Alumina Droplets: Observations and Characterization, *Mater. Sci. Eng. A*, 2007, **A456**, p 35-42.
192. T. Chraska and A.H. King, Transmission Electron Microscopy Study of Rapid Solidification of Plasma Sprayed Zirconia - part II. Interfaces and Subsequent Splat Solidification, *Thin Solid Films*, 2001, **397**, p 40-48.
193. M.W. Chase, *NIST-JANAF Thermochemical tables*, DTIC Doc. (1998)
194. W. Zhang and S. Sampath, A Universal Method for Representation of In-Flight Particle Characteristics in Thermal Spray Processes, *J. Thermal Spray Technol.*, 2009, **8**(23), p 34.
195. S.-W. Yao, J.-J. Tian, G.-J. Yang, C.-X. Li, X.-T. Luo and C.-J. Li, Understanding the Formation of the Limited Interlamellar Bonding in Thermal Spray Ceramic Coatings Based on the Intrinsic Bonding Temperature Concept, *J. Thermal Spray Technol.*, 2016, **25**, p 1617-1630.
196. E.-J. Yang, C.-J. Li, G.-J. Yang, C.-X. Li and M. Takahashi, Effect of Intersplat Interface Bonding on the Microstructure of Plasma-Sprayed $Al_2O_3$ Coating, *IOP Conf. Series: Mater. Sci. Eng.*, 2014, **61**, p 012022.
197. J. Knuuttila, S. Ahmaniemi and T. Mantyla, Wet Abrasion and Slurry Erosion Resistance of Thermally Sprayed Oxide Coatings, *Wear*, 1999, **232**, p 207-212.
198. S.-W. Yao, G.-J. Yang, C.-X. Li and C.-J. Li, Improving Erosion Resistance of Plasma-Sprayed Ceramic Coatings by Elevating the Deposition Temperature Based on the Critical Bonding Temperature, *J. Thermal Spray Technol.*, 2018, **27**(1-2), p 25-34.
199. S. Sampath, X.Y. Jiang, J. Matejicek, A.C. Leger and A. Vardelle, Substrate Temperature Effects on Splat Formation, Microstructure Development and Properties of Plasma Sprayed Coatings Part I: Case Study for Partially Stabilized Zirconia, *Mater. Sci. Eng. A*, 1999, **A272**, p 181-218.

200. A.H. Pakseresht, M.R. Rahimipour, M.R. Vaezi and M. Salehi, Effect of Splat Morphology on the Microstructure and Dielectric Properties of Plasma Sprayed Barium Titanate Films, *Appl. Surf. Sci.*, 2015, **324**, p 797-806.
201. S.-L. Zhang, C.-J. Li, C.-X. Li, G.-J. Yang and M. Liu, Atmospheric Plasma-Sprayed $La_{0.8}Sr_{0.2}Ga_{0.8}Mg_{0.2}O_3$ Electrolyte Membranes for Intermediate-Temperature Solid Oxide Fuel Cells, J. Mater. Chem., 2015, A 3, p 7535-7553.
202. C.-J. Li, Y. Li, G.-J. Yang and C.-X. Li, Evolution of Lamellar Interface Cracks during Isothermal Cyclic Test of Plasma-Sprayed 8YSZ coating with a columnar structured YSZ interlayer, *J. Thermal Spray Technol.*, 2013, **22**(6), p 1374-1382.
203. V. Viswanathan, G. Dwivedi, S. Sampath and T. Troczynski, Engineered Multilayer Thermal Barrier Coatings for Enhanced Durability and Functional Performance, *J. Am. Ceram. Soc.*, 2014, **97**, p 2770-2778.
204. Y.-P. Wang, J.-T. Gao, J.-H Li, C.-J. Li and C.-X. Li, Preparation of Bulk-Like $La_{0.8}Sr_{0.2}Ga_{0.8}Mg_{0.2}O_{3-d}$ Coatings for Porous Metal-Supported Solid Oxide Fuel Cells via Plasma Spraying at Increased Particle Temperatures, *Int. J. Hydrog. Energy*, 2021, **46**, p 32655-32664.